NISTIR 7081

Analysis of Pool Fires in Large Multi-Level Halls with the CFAST and FDS Fire Codes

Monideep Dey

U. S. DEPARTMENT OF COMMERCE
Technology Administration
National Institute of Standards
and Technology
Gaithersburg, MD 20899

NIST
National Institute of Standards and Technology
Technology Administration
U.S. Department of Commerce

NISTIR 7081

Analysis of Pool Fires in Large Multi-Level Halls with the CFAST and FDS Fire Codes

Monideep Dey

U. S. DEPARTMENT OF COMMERCE
Technology Administration
National Institute of Standards
and Technology
Gaithersburg, MD 20899

December 2003

U.S. DEPARTMENT OF COMMERCE
Donald L. Evans, Secretary

TECHNOLOGY ADMINISTRATION
Phillip J. Bond, Under Secretary for Technology

NATIONAL INSTITUTE OF STANDARDS
AND TECHNOLOGY
Arden L. Bement, Jr., Director

Abstract

The analysis presented in this report was conducted for Benchmark Exercise # 2, Part II in the International Collaborative Fire Model Project (ICFMP). The analysis was conducted with CFAST Version 3.1.6, a zone model, and FDS Version 2, a computational fluid dynamic model developed by the National Institute of Standards and Technology. The objective of the second benchmark exercise was to examine scenarios that are more challenging for zone models, in particular to fire spread in a multi-level large volume representative of turbine halls in nuclear power plants. FDS, including its output processor Smokeview, provides a comprehensive tool to examine the phenomena involved in the scenarios, specifically for examining the flow patterns through the hatches and ventilation systems. CFAST is a computationally efficient tool, providing the ability to determine solutions to problems within minutes; however, modeling vertical flow through horizontal vents in CFAST posed a challenge. Techniques are available to overcome this challenge. Bounding analyses of such scenarios with a zone model is also an option available to users. The ventilation in the scenarios examined significantly affects the flows, temperature, and other conditions in the compartments. The target temperatures are lower for ventilated conditions. Natural ventilation is more effective in preventing adverse compartment conditions for material targets and the human operator for the ventilation specifications given for the benchmark exercise. The codes predicted that the beam and cable targets would not reach damage temperatures for the scenarios examined.

Table of Contents

List of Figures

Executive Summary

The analysis presented in this report was conducted for Benchmark Exercise # 2, Part II in the International Collaborative Fire Model Project (ICFMP). The analysis was conducted with CFAST Version 3.1.6, a zone model, and FDS Version 2, a computational fluid dynamic model (CFD) developed by the National Institute of Standards and Technology. The objective of the second benchmark exercise was to examine scenarios that are more challenging for zone models, in particular to fire spread in a multi-level large volume representative of turbine halls in nuclear power plants.

FDS, including Smokeview, provides a comprehensive tool to examine the phenomena involved in the scenarios. The tools were useful in deriving interesting observations regarding the flow patterns through the hatches and ventilation systems. Such observations of flow and ventilation conditions which affect the thermal and smoke environment in a compartment cannot be derived intuitively, but only through such CFD analysis.

The specification of the grid size poses a challenge for FDS calculations. Ideally, a grid of 10 cm or less is optimal for simulating the large eddies in FDS. However, since some compartments modeled can be quite large, it would have been computationally expensive to use such a fine grid size. Also, FDS adjusts the size of the target which is used in the flow calculations to the minimum grid dimensions specified for the problem, if the target dimension is smaller than the grid size specified. This assumption by the code may affect the flow conditions, and therefore the calculated thermal environment around the targets. At the time the analysis was conducted, Version 3 of FDS which includes the capability to use multi-blocking, a term used to describe the use of more than one rectangular mesh in a calculation, was not available. This new version of FDS addresses several of the issues related to grid size.

CFAST is a computationally efficient tool, providing the ability to determine solutions to problems within minutes. Updating and improving the user interface and documentation will make the code even more effective and efficient. Modeling vertical flow through horizontal vents in CFAST (a zone model) posed a challenge. Firstly, since a zone model is a lumped model for each compartment, it is not possible to represent horizontal vents at different locations in the compartment. All horizontal vents have to be combined and represented by one vent, or a specific vent needs to be chosen for analysis while ignoring others that may not have an effect on compartment conditions. This assumption could be limiting when two or more vents interact and affect the flow pattern in the compartment. Techniques are available to overcome this challenge. Bounding analyses of such scenarios with a zone model is also an option available to users.

The ventilation in the scenarios examined significantly affects the flows, temperature, and other conditions in the compartments. The target temperatures are lower for ventilated conditions. Natural ventilation is more effective in preventing adverse compartment conditions for the material targets and the human operator for the ventilation specifications given for the benchmark exercise. The beam targets do not reach damage temperatures for the scenarios

examined. The cable targets are also not damaged, even considering surface temperatures.

The CFAST and FDS fire models used in this benchmark analysis have had limited validation for the types of scenarios examined, specifically for flow through hatches. Cooper's correlation that is used in CFAST for predicting vertical flow through horizontal vents has not been verified or validated. Further verification and validation of the submodel for vertical flow in horizontal vents in CFAST will be beneficial. Although, FDS has been validated (i.e. compared with experimental data) for several experiments conducted in large facilities, it would be beneficial to validate FDS for the specific types of scenarios examined here. Specific parameters that would benefit from comparison with experimental data are pressure in the compartments; and flow through the hatches, side vents in the lower and upper compartments, and roof vents. It will be beneficial to conduct tests to provide data for the validation of both codes to add confidence in their use for regulatory applications.

Acknowledgments

The author acknowledges the extensive efforts of Stewart Miles, Building Research Establishment, UK for developing the specification and conducting the benchmark exercise discussed in this report. The author also acknowledges the advice and consultation on the FDS code provide by Kevin McGrattan of the Building Fire Research Laboratory, National Institute of Standards and Technology (BFRL/NIST). The data presented for mass and heat flows for the vents and hatches for the benchmark analysis was provided by Kevin McGrattan using FDS 3 (beta-test version). The author also acknowledges the advice and consultation on the CFAST code by Walter Jones, BFRL/NIST.

1 Introduction and Specification of Problem

1.1 Introduction

The analysis presented in this report was conducted for Benchmark Exercise # 2, Part II in the International Collaborative Fire Model Project (ICFMP). The analysis was conducted with CFAST Version 3.16, a zone model [Jones et al, 2000], and FDS Version 2, a computational fluid dynamic model [McGrattan et al, 2001].

In October 1999, the U.S. Nuclear Regulatory Commission and the Society of Fire Protection Engineers organized a planning meeting of international experts and practitioners of fire models to discuss the evaluation of numerical fire models for nuclear power plant applications [Dey, 2000]. Following this meeting an international collaborative project was set up with a view to sharing knowledge and resources from various organizations and to evaluate and improve the state of the fire modeling methods and tools for use in nuclear power plant fire safety.
The first task of the collaborative project was to undertake a benchmark exercise to evaluate the current capability of fire models to analyze the hazard associated with cable tray fires of redundant safety systems in nuclear power plants. The exercise involved a series of hypothetical scenarios to predict cable damage inside an emergency switchgear room. Target cable damage was predicted to be unlikely in almost all cases studied [Dey, 2002].

The objective of the second benchmark exercise was to examine scenarios that are more challenging for zone models, in particular to fire spread in a multi-level larger volume representative of turbine halls in nuclear power plants. The specification of the benchmark exercise [Miles, 2002] provided to participants is included below.

Following this, the report initially provides a discussion of key input parameters and assumptions for the analysis of the scenarios in the benchmark exercise. This is followed by a presentation of the results of the analysis and a discussion of the general conclusions and recommendations. The capabilities and limitations of the two codes for analyzing the scenarios in the exercise are highlighted and recommendations for additional code validation are provided.

1.2 Specification of Problem

The following provides some key elements for the specification of the problem. The reader is encouraged to review the full specification [Miles, 2002] for further details, specifically for the material and fire properties used for the analysis.

Part II of Benchmark Exercise # 2 included three cases for which experimental measurements do not exist, but extended the scope of the benchmark exercise to examine the effect of a bigger fire and larger floor area representative of a hydrocarbon pool fire in a real turbine hall. Three scenario cases (Cases 1, 2 & 3) set inside a rectangular building with dimensions comparable to those of a real turbine hall are analyzed. Targets have been added to Part II to allow the onset of

damage to be studied. The fire size has been chosen to produce temperatures that may be capable of damaging equipment or cables.

Geometry

Figure 1 shows the dimensions of the building. As shown in Figure 2, the building is divided into two levels (decks) connected by two permanent openings (hatches). Although many turbine halls contain three decks, it was been decided that modeling two decks is sufficient for the benchmark exercise. Figure 3 shows the exact location of the internal ceiling and the two open hatches (each 10 m by 5 m in size).

Material Properties

The floor, lower walls (lower deck) and internal ceiling (separating the two decks) are constructed from concrete (see Miles, 2002 for thermal properties) with a thickness of 0.15 m. The upper walls (upper deck) and ceiling are constructed from steel, which for the benchmark exercise is to be modeled simply as sheet metal of thickness 0.002 m.

Ventilation Conditions

Cases 1, 2, and 3 have different ventilation conditions, covering nearly-sealed conditions, natural ventilation conditions and a combination of natural and mechanical ventilation. For Case 1, the hall is nearly sealed, with two infiltration openings each of dimension 1 m x 1 m. Both openings are located at floor level on the lower deck. One is in the westwall, with its centre located at co-ordinates (x = 0, y = 25, z = 0.5), and the other is in the east wall at co-ordinates (x = 100, y = 25, z = 0.5).

Case 2 includes natural ventilation. It is assumed for the benchmark exercise that the complete set of smoke exhaust vents at roof level is open for the full duration of the scenario. There are 36 smoke exhaust roof vents at roof level (upper deck), each with dimensions 3 m (x direction) by 1.5 m (y direction). The roof vents are arranged symmetrically in a 9 by 4 array in the x-y directions with a 10 m spacing between the centre of the vents (in each direction). There is thus a distance of 10 m between the centre of the outer vents and the edge of the roof. For Case 2, there is a complimentary set of 24'make-up vents in the side walls, each with dimensions of 2 m x 2 m, again assumed to be open for the full duration of the scenario. There are 12 vents located at floor level on the lower deck and 12 at floor level on the upper deck (just above the internal ceiling), i.e. the centre of the vents are located at z = 1 m and z = 11 m respectively. The 12 vents (at each deck) are distributed around the building with two vents in each of the west and east walls and four vents in each of the south and north walls. In each wall (at each deck) a distance of 20 m separates the centre of the vents. Hence there is a distance of 20 m from the centre of the outer most vents to the edge of the south and north walls, and a corresponding distance of 15 m to the edge of the west and east walls.

Case 3 is a variation on Case 2, with the 36 roof level smoke exhaust vents replaced by a set of

36 mechanical vents, each with dimensions of 1 m x 1m. The centres of the mechanical vents are at the same locations as those of the natural smoke exhaust vents in Case 2. For case 3, it is assumed that a fixed total mechanical extraction rate of 194.4 m^3s^{-1} is maintained for the full duration of the scenario (corresponding to 7 air-changes-per-hour). The individual mechanical extraction rate for each vent is 5.4 m^3s^{-1}. For the purpose of the benchmark exercise, it is assumed that the make-up air is supplied by natural ventilation openings in the four walls. For Case 3 the same 24 natural ventilation wall openings should be considered as for Case 2.

Fire source

For all three cases, the fire source is assumed to be lube oil burning in a dike (tray) with dimension 7 m by 7 m, located at the centre of the lower deck. It should be assumed that the surface of the fuel is 1 m above the floor.

The mass release rate of the pool fire grows from zero to a steady value 1.66 kg s^{-1} as follows,

$$\dot{m}_f = \alpha . t^2$$

Here t is the time in seconds from the start of the fire, and α is a constant with a value 4.611×10^{-6} kg s^{-3}. This value is derived from an assumed NFPA ultra fast t-squared growing fire. The above equation defines the mass release rate for the first 10 minutes, at which time it reaches the steady-state at a value of 1.66 kg s^{-1} which is maintained for the next 10 minutes (giving 20 minutes total duration). It is assumed that the fuel surface covers the complete area of the 7 m by 7 m dyke for its full duration, i.e. the mass release rate per unit area increases according to the same function as in the equation above.

The chemical and thermal properties for the combustion of lube oil can be found in the full specification.

Energy is released according to

$$Q = m_f \Delta H_c$$

where ΔH_c is the heat of combustion.

Targets

To make Part II relevant to practical applications, three cable targets have been introduced, similar to the first benchmark exercise. Each cable is a 50 mm (0.05 m) diameter power cable, assumed to consist entirely of PVC. The thermal properties of the cable material are the same as in the first benchmark exercise [Dey, 2002a]. As for the first benchmark exercise, the onset of cable damage is when the centerline temperature reaches 200 °C.

Two structural beam targets are also included. To simplify the modeling, each 'beam' is approximated as a horizontally orientated rectangular slab of steel with cross-sectional dimensions of 0.15 m wide (x co-ordinate direction) and 0.006 m thick (z co-ordinate direction). Material properties for the 'beam' targets, where the conductivity, density and specific heat correspond to steel (0.5% carbon) at 20°C can be found in the full specification. It was assumed for the purpose of this exercise that property values are temperature independent. A damage temperature of 538 °C is assumed.

Figure 4 shows the locations of the three cable targets and the two 'beam' targets. The cables extend the full length of the hall (x direction), and the 'beam' targets extend the full width (y direction). The centre-lines of the three cables are 1 m from the south wall, and 9 m, 15 m and 19 m above the floor of the lower deck respectively. The 'beam' targets are located half-way along the length of the hall (x = 50 m). The centre-line of one 'beam' is 0.5 m below the ceiling of the lower deck (the internal ceiling), and the second 'beam' is 0.5 m below the ceiling of the upper deck (the roof).

Additionally, there is a ‘human target’, located 1.5 m above floor level (the internal ceiling) at the centre of the upper deck, i.e. at co-ordinates (x = 50, y = 25, z = 11.5).

Summary of Exercise Cases

The three cases to be simulated are summarized below.

Summary of Cases

Case 1		*Case 2*
Nearly-sealed. Two *1 m* x *1 m* openings.		Natural ventilation. 36 roof vents. 24 make-up wall vents.
Case 3		
Mechanical (extract) and natural ventilation. *194.4* $m^3 s^{-1}$ mechanical exhaust ventilation (divided evenly between 36 roof vents) 24 make-up wall vents.		

2 Input Parameters and Assumptions

2.1 Modeling Horizontal Vents in Zone Models

Modeling horizontal vents in zone models posed a challenge. Firstly, since a zone model is a lumped model for each compartment, it is not possible to represent horizontal vents at different locations in the compartment. All horizontal vents have to be combined and represented by one vent, or a specific vent needs to be chosen for analysis while ignoring others that may not have an effect on compartment conditions. In this benchmark exercise, the two hatches were combined and modeled as one horizontal vent in the compartment. This is a limitation because there are important flow phenomena which differ in the two hatches, as discussed later.

The modeling of vertical flow through a horizontal vent is complex and difficult. A non-zero cross vent pressure difference will lead to unidirectional flow from the higher to the lower pressure side. However, an unstable configuration develops when the fluid densities are reversed, i.e., the hotter gas in the lower compartment is underneath the cooler gas in the upper compartment. This will lead to flow from the lower compartment to the upper compartment. This phenomenon is difficult to model.

In CFAST (Jones, 2000), Cooper's algorithm is used for computing mass flow through ceiling and floor vents. There are two components to the flow. The first is net flow dictated by a pressure difference. The second is an exchange flow based on the relative densities of gas. CFAST also attempts to model flow shedding for the bidirectional flow, i.e., flow from the hot gas layer (HGL) in the lower compartment to the HGL in the upper compartment will shed in the upper compartment lower layer; flow from the upper compartment lower layer to the lower compartment lower layer will shed in the HGL in the lower compartment. Selection criteria in CFAST based on the pressure and density differences determine the direction of the flows.

Cooper's correlation for vertical flow in horizontal vents has not been verified or validated [Dey, 2002]. Some comparisons with results from tests conducted at the U.S. Navy's test ship, ex-USS Shadwell, have been made. However, the tests were conducted for a different purpose, other than verifying and validating CFAST, and did not provide all the necessary data to verify and validate the flow submodel.

2.2 Target Model

A detailed heat transfer model for a cable tray will be fairly complex. Cable trays generally have a number of cables bundled together in layers, and most cables consist of several conductors. Cables configured in a single layer will get damaged and ignite at a lower flux than cables in a multilayer configuration because the flux to a single layer will not be shielded by cables above

that layer. The CFAST or FDS codes currently do not include a target model of such complex cable configurations. For simplicity, the target in the benchmark exercise was specified to be one power cable conservatively composed only of PVC. The CFAST and FDS codes have a simple one-dimensional slab model for targets. They do not currently include a 1-D radial model to approximate radial heat transfer in cables. The cable targets are represented as rectangular slabs, the slabs were assumed to be oriented horizontally with a thickness of 50 mm. A one-dimensional target model may not be adequate since the incident radiative flux would vary with the orientation of the slab. Also, the specification of the slab thickness, and selection of the criterion for cable damage (surface temperature versus centerline temperature) would be key to the success of a one-dimensional target model.

The heat transfer model in both CFAST and FDS are similar and include a 1-D conduction calculation for the specified thickness of the target. However, FDS adjusts the size of the target which is used in the flow calculations to the minimum grid dimensions specified for the problem, if the specified grid size is larger than the target dimension. For the benchmark exercise, a grid of 1 m x 1 m x 1 m was specified. Therefore, the targets were adjusted to blockages of 1 m x 1 m x length or width of the compartment. This assumption by the code will affect the flow conditions and therefore the thermal environment around the targets. However, the target is still assumed to be the specified dimensions in the 1-D heat transfer calculations executed in FDS.

2.3 Chemical Composition of Fuel

The problem specification included the H/C mass ratio, and the yields of CO and CO_2. These properties of the fuel were sufficient to complete the input data required for the combustion model [Jones, 2000] in CFAST which tracks the mass balances of species in the combustion process. In the FDS2, it is assumed that a single hydrocarbon fuel is being burned, with constant yields of CO and soot. The user needs to define the *ideal* stoichiometric coefficients for the fuel, O_2, CO_2 and H_2O, and yields for CO and soot. The data provided in the problem specification was not sufficient to uniquely define the chemical formula and molecular weight of the fuel that is needed to calculate the stoichiometric coefficients that are input to the FDS code. It was assumed that the fuel had the same composition as ethylene, C_2H_4, which has a H/C mass ratio of 0.17, as specified. A ratio of two H to one C atom (H/C mass ratio = 0.17) is typical in long chain hydrocarbons such as lube oil. The yields of CO and soot specified in the problem description were then used for the analysis.

2.4 Grid Resolution

The specification of the grid size posed a challenge for the FDS calculations. The optimal grid for simulating the large eddies in FDS must be determined. Although a grid of 10 cm may be adequate in this case, an even smaller grid generally may yield better results. However, since the compartment modeled was 100 m x 50 m x 20 m, it would have been computationally expensive

to use a fine grid size. As a rule of thumb, the computational time for FDS increases by a factor of 20 if one decreases the grid size by half in each coordinate. In order to minimize computational times, a grid of 1 m x 1 m x 1 m was used in the analysis. This provided about 7 grid cells across the fire which is expected to be adequate to resolve the fire. Version 3 of FDS [McGrattan, 2002] which includes the capability to use multi-blocking, a term used to describe the use of more than one rectangular mesh in a calculation, was not available at the time the analysis was conducted. A grid sensitivity analysis which provides useful information for CFD analyses was not conducted due to time constraints. The assumptions for the grid dimensions will affect the resolution of the fire and the flow around the targets, as discussed above.

2.5 Mixture Fraction Model in FDS

The FDS code includes a mixture fraction chemistry model [McGrattan, 2001]. The code is based on the assumption that large-scale convective and radiative transport phenomena can be simulated directly, but physical processes occurring at small length and time scales must be represented in an approximate manner. All species of interest are described in terms of a mixture fraction

$Z(\mathbf{x}, t)$. The form of the state relations between the species of interest and the mixture fraction, based on classical laminar diffusion theory, lead to a "flame sheet' model where the flame is a two dimensional surface embedded in a three dimensional space. Oxygen and fuel diffuse from areas of higher to lower concentrations and meet at the flame sheet where there is instantaneous and complete combustion. Multiple flames, such as those that would result from the pool fire in this benchmark exercise, is approximated by a single diffusion flame. The local heat release rate is computed from the local oxygen consumption rate at the flame surface, assuming that the heat release rate is directly proportional to the oxygen consumption rate, independent of the fuel involved. The mixture fraction at the flame surface, Z_f, is defined where the fuel and oxidizer simultaneously vanish. Z_f is around 0.05 for most hydrocarbon fuels. In the numerical algorithm, the local heat release rate is computed by first locating the flame sheet, then computing the local heat release rate per unit area, and finally distributing this energy to the grid cells cut by the flame sheet.

One assumption inherent in the mixture fraction model is that the combustion process is temperature independent, i.e. the state relations between the mass fraction of each species and mixture fraction is fixed. FDS currently includes some approximate techniques to account for this assumption when the oxygen concentration or temperature is too low to sustain combustion. For scenarios where the fire is under ventilated, the flame sheet will be extended to regions where the fuel and oxygen are at the ideal stochiometric ratios input to the code. However, this does not indicate the presence of combustion in those regions because the temperatures may not be high enough to sustain combustion.

3 Results of Analyses

3.1 Summary of Results

The ventilation in the scenarios examined significantly affects the flows, temperature, and other conditions in the compartments. The target temperatures are lower for ventilated conditions. Natural ventilation is more effective in preventing adverse compartment conditions for the material targets and human operator for the ventilation specifications given for the benchmark exercise. The beam targets do not reach specified damage temperatures for the scenarios examined. The cable targets are not damaged, even considering surface temperatures.

3.2 Qualitative Examination of Phenomena in Scenarios

Initially, the analysis of the scenarios with FDS is presented to provide a discussion of the key phenomena of interest. Figures 5 and 6 show the model of the compartment for Case 1 in FDS through the output processor of the code, Smokeview. The two hatches are shown along with the beam and cable targets in the upper and lower levels. The beam targets below the ceiling of the lower and upper compartments are designated as B1 and B2 respectively. The cable targets are designated as C1, C2, and C3 corresponding to the cable targets at a height of 9m in the lower compartment, and at 15 m and 19 m in the upper compartment. As indicated earlier, the cable and beam targets are shown as modeled in FDS for the flow calculations, i.e., 1 m x 1 m x length of cable or beam. Figure 5 also shows the vents (1 m^2) specified in FDS that model infiltration. The location of the fire in the center of the compartment is shown in Figure 6.

3.2.1 Case 1

Figure 7 shows a slice file of the temperature profile at the midpoint along the length of the compartment toward the end of the transient (t = 1083 s). The flow of hot gases from the lower to the upper compartment through Hatch 1 can be observed. The results of the simulation for this case shows that both the lower and the upper compartment is almost (~ 75-100 %) full of hot gases at the end of the transient. The average temperatures of the hot gases reach ~ 400-550 K and will be discussed further later and compared with temperatures achieved in the other cases.

Figure 8 is a vector plot of the flow patterns in the compartment at 600 s. The plot shows the velocity vectors in a plane in the compartment (which for this Figure is the midpoint along the width of the compartment). The velocity vector is shown by the arrows which are also color coded to indicate the temperature of the gas at that point. The significant upward flow of hot gases through Hatch 1 at up to 7 m/s is shown, as well as the high velocity of the flow through the infiltration openings. The Figure also shows that the beam target, B1, is exposed to the

plume flow from the fire. A slight tilt of the plume to the right is observed which will be discussed later.

Figure 9 shows another velocity vector plot at 600 s at a plane that intersects Hatch 2. It is interesting to note that the flow of hot gases is downward from the upper to the lower compartment. Intuitively, one might expect that the flow through Hatch 2 will also be upward. The high velocity of the fire plume gases causes an upward flow through Hatch 1 which pressurizes the upper compartment. The pressurization of the upper compartment then causes the flow through Hatch 2 to be downward. This flow phenomenon was confirmed by viewing particle files generated by FDS with Smokeview. Particles can be viewed which show the direction of the flow and smoke generated through the transient. The maximum flow velocity is approximately 1.4 m/s downward through Hatch 2 for Case 1.

Figure 10 shows a boundary file from Smokeview indicating the surface temperatures of the targets at ~ 1200 s in the upper compartment. The hottest areas of the beam and cable targets at ~ 415 K are indicated in black. The Figure shows that the hottest areas of the target are not necessarily right above the fire or hatch. For example, Figure 10 shows the hottest area of the target, B2, is slightly to the right of Hatch 1 due to the tilting of the hot gas plume as it flows through the hatch. However, it should be noted that it is not possible to pinpoint the exact location of the hotspot in the target with this analysis because the targets are modeled larger than actual to minimize the size of the grid. The size of the targets will modify flow in the vicinity of the targets and affect its temperature evolution.

Finally, Figure 11 shows an isosurface in the hot gas where the mixture fraction, $m_f = 0.05$ toward the end of the transient at ~ 920 s. As discussed earlier, this isosurface should not be interpreted as the flame sheet because the oxygen in this case is depleted toward the end of the transient (see Figure 24 discussed later) and the fire becomes under ventilated. The temperatures in the compartment, especially away from the fuel pool, are not high enough to sustain combustion and the fire will not spread through the compartment as the Figure may imply if incorrectly interpreted.

3.2.2 Case 2

Figure 12 shows the model of the compartment for Case 2. The side natural vents in both compartments and the natural roof vents are shown.

Like Figure 7 for Case 1, Figure 13 similarly shows a slice file of the temperature profile at the midpoint along the length of the compartment toward the end of the transient (t = 1083 s) for Case 2. The results of the simulation for this case shows that lower compartment is only ~ 30 % full of hot gases, and the upper compartment has minimal accumulation of hot gases (~ 20 % full) at the end of the transient. The temperature environment for Case 2 with natural ventilation

is much less severe than in Case 1 with no ventilation at the end of the transient. The average temperatures of the hot gases reach ~ 280-350 K and will be discussed further later with comparisons with temperatures achieved in the other cases. Figure 14 shows a velocity vector plot of the flow patterns in the compartment at 1026 s in a plane along the length of the compartment that intersects the fire, Hatch 1, and a set of roof vents. The high upward velocity component (w-vel) of the gases through the roof vents at ~ 8 m/s is illustrated by the Figure. In this Figure the velocity vectors are coded with the upward component (w-vel) of velocity.

Figure 15 shows a slice file of the pressure profile at the midpoint along the length of the compartment toward the end of the transient (t = 1200 s) for Case 2. The Figure shows that the lower regions of both the upper and lower compartments are maintained at a negative pressure of about - 20 to 5 Pa through out the transient causing inflow from all the side vents and outflow through the roof vents. The pressure distribution for Case 1 is mostly uniform because the compartment is almost sealed. The pressure development for Case 1 is shown later in Figure 23. Figure 16 shows a velocity vector plot of the flow patterns in the compartment at 600 s in a plane along the length of the compartment that intersects set of side and roof vents. The flow shown in the Figure is in from side vents both in the lower and upper compartments, and out from the roof vents.

3.2.3 Case 3

Figure 17 shows the model of the compartment for Case 3. The side natural vents are the same as for Case 2, but the roof vents are mechanical with smaller openings.

Like Figures 7 and 13 for Cases 1 and 2, Figure 18 similarly shows a slice file of the temperature profile at the midpoint along the length of the compartment toward the end of the transient (t = 1083 s) for Case 3. The results of the simulation for this case shows that the lower compartment is about 30 % full of hot gases, and the upper compartment is 80 % full of hot gases toward the end of the transient. The temperature environment for Case 3 with natural side vents and mechanical roof vents is less severe than Case 1 with no ventilation, but more severe than Case 2 with all natural vents at the end of the transient. This indicates that natural ventilation is more effective in decreasing the severity of the thermal environment for the specified configuration. The average temperatures of the hot gases reach about 350 - 390 K and will be discussed further later with comparisons with temperatures achieved in the other cases.

Figure 19 shows a slice file of the pressure profile at the midpoint along the length of the compartment toward the end of the transient (t = 1200 s) for Case 3. The Figure shows that the lower region of the lower compartments is maintained at a negative pressure of ~ -10 to - 20 Pa through out the transient but the pressure in the lower region of the upper compartment becomes positive at the end of the transient. Therefore, flow is into the compartment from the side vents in the lower compartment, but out of the compartment from the side vents in the upper compartment toward the end of the transient. This phenomena is illustrated in Figure 20 which

shows a velocity vector plot of the flow patterns in the compartment at 1200 s in a plane along the length of the compartment that intersects set of side and roof vents. The flow is in from the side vents in the lower compartment, but out of the compartment from the side vents in the upper compartment at the end of the transient.

Finally, Figure 21 shows another velocity vector plot at 1200 s at a plane that intersects Hatch 2. The flow of hot gases is noted to be upward from the lower to the upper compartment for Case 3. A similar flow pattern was noted for Case 2. In Cases 2 and 3, the flow through the roof vents prevents the pressurization of the upper compartment and allows the flow through Hatch 2 to be upward.

3.2.4 Summary of Observations and Conclusion

Interesting observations regarding the flow patterns indicate that flow is upward through Hatch 1 but downward through Hatch 2 in Case 1. The flow is upward for both Hatches 1 and 2 in Cases 2 and 3. The pressure in the upper compartment becomes positive toward the end of the transient in Case 3 which results in outflow from the side vents in that compartment. Such observations of flow conditions which affect the thermal environment in a compartment cannot be made intuitively, but can only be determined through such analysis. FDS, including Smokeview, provides a comprehensive tool to examine the phenomena involved in the scenarios.

3.3 Quantitative Results

3.3.1 Case 1

Figure 22 shows the heat release rate input to both the CFAST and FDS codes. The HRR is input directly to CFAST which is ramped up to 63.5 MW in 600 s. The HRR profile is also input into FDS, however, the actual input used by FDS is calculated using the mixture fraction model. As discussed earlier, the mixture fraction model calculates a flame sheet where the mixture fraction, $m_f = 0.05$, i.e. where the fuel and oxygen are at an ideal stochiometric ratio. FDS then spreads the total heat release specified across the cells intersected by the flame sheet. This translation results in some discrepancy between the heat release rate specified by the user and that used by FDS in predicting the thermal environment.

The hot gas layer development (HGL) predicted by CFAST is shown in Figure 23. Similar to predictions by FDS discussed above, CFAST predicts that both the lower and upper compartments are filled with hot gases at the end of the transient.

The predicted gas temperatures for Case 1 are compared in Figure 24. The temperatures predicted by CFAST shown are the *average* temperature for the lower and upper compartments. The maximum temperatures predicted at the end of the transient by CFAST is ~ 502 K for the

lower compartment, and ~ 371 K for the upper compartment. The temperature profiles predicted by FDS at the *specific locations* T2.8 (below the ceiling of the lower compartment), T2.19 (below the ceiling of the upper compartment, and at the human target (1.5 m above the floor at center of upper compartment) are shown in the Figure. The temperature of the hot gas at the human target reaches ~ 425 K, 132 K above ambient conditions.

Figure 25 shows the pressure development for Case 1. The peak pressure predicted by FDS is ~ 1637 Pa (at ~ 910 s), compared to ~ 698 Pa (at 560 s) predicted by CFAST. The prominent double peak in the pressure profile predicted by CFAST is due to reversals of flow through the hatches. The hatch flow dynamics is discussed later when the flows through the hatches are reported. The pressure reported from FDS is at T2.1, however, the pressure distribution in the compartment for this case is almost uniform. The peak pressure predicted by FDS is higher than that predicted by CFAST by a factor of 2.4. The corresponding flows from the infiltration openings predicted by CFAST and FDS are shown in Figure 26. The peaks in the flows correspond to the pressure peaks in Figure 25.

Figure 27 presents the oxygen concentration in the compartment during the transient. The predictions of average oxygen concentration in the upper and lower compartments by CFAST, and the concentrations at points T2.8 and T2.19 by FDS are shown. The minimum concentration predicted by CFAST in the lower compartment HGL and by FDS at T2.8 is ~ 13.6 %. The predictions of oxygen concentration in the upper compartment between CFAST and FDS are also similar. The oxygen concentration in the upper compartment is less than the lower compartment due to the entrainment of air by the plume hot gas as it flows through Hatch 1. The predictions indicate that the oxygen concentration in the lower compartment approach the lower oxygen limit (LOL); therefore, the fire will be under ventilated toward the end of the transient. This is illustrated by Figure 11 which was discussed earlier.

Figure 28 shows the average soot density in the HGLs of the upper and lower compartments predicted by CFAST, and the specific density at the human target predicted by FDS. The soot density in the upper compartment predicted by CFAST at the end of the transient is ~ 0.34gm/m^3. The soot density predicted by FDS at the human target at the end of the transient is ~ 0.56 gm/m^3.

For clarity, a discussion of the parameters and definitions used in the calculation of visibility is provided here since there are a number of different definitions used by practicing engineers that can be confusing to the user.

The most useful quantity for assessing visibility in a space is the *light extinction coefficient,* ***K*** [Mulholland, 1995]. The intensity of monochromatic light passing a distance L through smoke is attenuated according to Bouguer's law:

$I/I_0 = e^{-KL}$

When expressed in terms of base 10 the equation is

$I/I_0 = 10^{-DL}$

The quantity D is defined as the optical density (OD) per meter, and D = K/2.3.

The extinction coefficient, $\boldsymbol{K}$, is an extensive property and can be expressed as the product of an extinction coefficient per unit mass, $\boldsymbol{K_m}$, and the mass density of the smoke particulate, m.

$K = K_m m$

The specific extinction coefficient, $\boldsymbol{K_m}$, depends on the size distribution and optical properties of the smoke particulate. Seader and Einhorn [Seader, 1976] obtained $\boldsymbol{K_m}$ values of 7600 m^2/kg for smoke produced during flaming combustion of wood and plastics. Both, the CFAST and FDS codes use this value for $\boldsymbol{K_m}$ as default input values.

Estimates of visibility through smoke can be made using the equation

$S = C/K$

where C is a nondimensional constant characteristic of the type of object being viewed through the smoke. C has been measured to be 8 for a light-emitting sign, and 3 for a light-reflecting sign [Mulholland, 1995].

The FDS code can output the visibility as defined above for a value of C which is input to the code. The CFAST code outputs the optical density (OD) per meter as defined above from which the user can calculate the visibility.

Figure 29 shows the visibility for a light-reflecting sign in the HGL in the upper and lower compartments from CFAST, and at the human target by FDS. The visibility is predicted to approach 10 m at ~ 390 s in the HGL of the upper compartment by CFAST, and at ~ 530 s at the human target by FDS.

Figure 30 shows the evolution of the surface temperatures in the targets predicted by CFAST. The temperatures for targets B1 and C1 are predicted to reach 445 K and 421 K respectively at the end of the transient, while the other targets are predicted to not experience any significant increase in temperature. Figure 31 shows the evolution of the surface temperatures in the targets

predicted by FDS. The temperatures for targets B1 and C1 are predicted to reach 543 K and 431 K respectively at the end of the transient. FDS predicts the maximum temperature of C3 to reach 470 K, which is higher than the maximum temperature of C1. The temperatures reported are at the center along the lengths of the cable and beam targets. FDS predicts a higher temperature for B1, compared to CFAST, because it includes simulation of the plume and ceiling jet flows that affect B1. Similarly, FDS predicts higher maximum temperature for C3, compared to CFAST, which is exposed to the plume gases going through Hatch 1. Figures 26 and 27 show the corresponding total fluxes to the targets predicted by the CFAST and FDS codes.

The cable damage temperature was specified at 473 K at the centerline, and the beam damage temperature was at 811 K at the surface. FDS and CFAST do not provide the centerline temperatures as output information. The beam surface temperatures do not reach the specified damage temperature, and the cable surface temperatures do not exceed the specified damage temperature for the cable centerline.

Figure 34 shows the mass flows through the Hatches predicted by CFAST and FDS. The corresponding heat flows through the hatches predicted by FDS is shown in Figure 35. As indicated earlier, the hatches are combined for the CFAST zone model. The flow upward through Hatch 1, and downward through Hatch 2 predicted by FDS and discussed earlier is shown in the Figure. The flow predicted through Hatch 1 and 2 by FDS approach 30 kg/s and -70 kg/s, respectively. The heat flows predicted by FDS approach 10 MW and - 5 MW through Hatches 1 and 2. The heat flow through Hatch 1 is larger due to its proximity to the fire.

The various combinations of flows through the hatch from the upper and lower compartment upper and lower layers predicted by CFAST is also shown in Figure 34. As discussed earlier, CFAST attempts at modeling flow shedding for bi-directional flow which is predicted for this case, i.e., some flow from the hot gas layer (HGL) in the lower compartment to the HGL in the upper compartment will be retained in the upper compartment lower layer, flow from the upper compartment lower layer to the lower compartment lower layer will shed in the HGL of the lower compartment. Selection criteria in CFAST based on the pressure and density differences determine the direction of the flows. The figure illustrates the difficulty of implementing this type of model with selection criteria. The selection criteria which determine the direction of the flows result in discontinuities (shown in figure) that are not realistic.

As mentioned earlier, Cooper's correlation that is used in CFAST for predicting vertical flow in horizontal vents has not been verified or validated [Dey, 2002]. Some comparisons with results from tests conducted at the U.S. Navy's test ship, ex-USS Shadwell, have been made. However, the tests were conducted for a different purpose, other than verifying and validating CFAST, and did not provide the necessary data to verify and validate the hatch flow submodel. Further verification and validation of the submodel for vertical flow in horizontal vents in CFAST will be beneficial.

Even assuming the correlation for vertical flow through horizontal flow in CFAST was verified and validated, the limitation of a zone model in being able to simulate only one vertical opening limits its validity for analyzing Case 1. As described earlier, the flow through the hatches predicted by FDS is unidirectional because the two hatches are inter-connected in the flow dynamics. The high velocity of the fire plume gases causes an upward flow through Hatch 1 which pressurizes the upper compartment. The pressurization of the upper compartment then causes the flow through Hatch 2 to be downward. FDS does not predict the flows through Hatches 1 and 2 to be bidirectional.

It should be noted here that others have been successful in using zone models to predict vertical flows through horizontal vents [Rockett, 1992]. The reader is encouraged to review these other techniques for simulating vertical flows through horizontal vents in zone models. These methods are not further applied or evaluated here due to time and resource constraints.

3.3.2 Case 2

Figure 36 shows the heat release rate input to both the CFAST and FDS codes. In this case, the heat release rate used by FDS closely follows the input HRR.

The hot gas layer development (HCL) predicted by CFAST is shown in Figure 37. Similar to predictions by FDS discussed above, CFAST predicts that both the lower and upper compartments are only ~ 20 % filled with hot gases at the end of the transient. The natural roof and side vents result in a less severe thermal environment for Case 2, compared to Case 1.

The predicted gas temperatures for Case 2 are compared in Figure 38. The temperatures predicted by CFAST shown are the *average* temperature for the lower and upper compartments. The maximum temperatures predicted at the end of the transient by CFAST is ~ 525 K for the lower compartment, and ~ 361 K for the upper compartment. The temperature profiles predicted by FDS at the *specific locations* T2.8, and at the human target (1.5 m above the floor at center of upper compartment) are shown in the Figure. There is no appreciable increase in the temperature of the hot gas at the human target.

Figure 39 shows the pressure development for Case 2. The pressure predicted by FDS at T2.1 becomes negative to ~ -15 Pa as the flow through the roof and side vents develop, as discussed above. The negative pressures on the floor in the lower and upper compartments due to the vent flows predicted by CFAST are much larger, at - 67 Pa and - 86 Pa respectively.

Figure 40 shows the average soot density in the HGLs of the upper and lower compartments predicted by CFAST, and the specific density at the human target predicted by FDS. The soot density in the upper compartment predicted by CFAST at the end of the transient is ~

0.21gm/m^3. The soot density predicted by FDS at the human target at the end of the transient is only ~ 0.35gm/m^3 due to the decreased development of the HGL at the human target.

Figure 41 shows the visibility for a light-reflecting sign in the HGL in the upper and lower compartments from CFAST, and at the human target by FDS. The visibility is predicted to approach 10 m at ~ 250 s in the HGL of the upper compartment by CFAST. The visibility at the human target is predicted to level at ~ 10 m by FDS indicating favorable conditions even at the end of the transient.

Figure 42 shows the evolution of the surface temperatures in the targets predicted by CFAST. The temperatures for targets B1 and C1 are predicted to reach 632 K and 440 K, respectively, at the end of the transient, while the other targets are predicted to not experience any significant increase in temperature. The temperature for B1 for Case 2 should be less than for Case 1 at 421 K. Therefore, the reported temperature of 632 K is unexplained. Figure 43 shows the evolution of the surface temperatures in the targets predicted by FDS. The temperatures for targets B1 and C1 are predicted to reach 666 K and 366 K, respectively, at the end of the transient. FDS predicts the maximum temperature of C3 to reach 340 K, which in this case is less than the maximum temperature of C1. In Case 2, C3 is in the vicinity of the roof vents which exhausts the hot gases and therefore in a cooler environment. The beam surface temperatures do not reach the specified damage temperature of 811 K, and the cable surface temperatures do not exceed the specified damage temperature 473 K for the cable centerline.

Figure 44 shows the mass flows through roof and side vents predicted by CFAST and FDS. The flow through the roof and side vents predicted by CFAST (~ 906 kg/s) is almost twice that predicted by FDS (~ 556 kg/s). The development of the flow is simulated by FDS, whereas CFAST predicts an instantaneous development of the flow due to the assumptions embedded in the zone model.

Figure 45 shows the mass flows through the hatches predicted by CFAST and FDS. The corresponding heat flows through the hatches predicted by FDS is shown in Figure 46. As indicated earlier, the hatches are combined for the CFAST zone model. This assumption which is necessary in CFAST does not result in a significant limitation for Case 2, as for Case 1, because the flow through both the hatches are upward from the lower to upper compartments in Case 2. Figure 45 shows that the upward flow predicted through both Hatch 1 and 2 by FDS which levels at ~ 150 kg/s. The total hatch flow predicted by CFAST is ~ 425 kg/s compared to ~ 300 kg/s by FDS. The heat flows through the hatches predicted by FDS approach 22 MW each, indicating ~ 70 % of the heat is transferred from the lower to the upper compartment in this scenario.

3.3.3 Case 3

The hot gas layer development (HGL) predicted by CFAST is shown in Figure 47. Similar to predictions by FDS discussed above, CFAST predicts that the lower compartment is ~ 30 % of hot gases, and the upper compartment is ~ 85 % full of hot gases toward the end of the transient. The mechanical roof vents (flowrate is kept constant) result in a less favorable thermal environment in Case 3, particularly in the upper compartment, as compared to Case 2 with larger natural roof vents.

The predicted gas temperatures for Case 3 are compared in Figure 48. The temperatures predicted by CFAST shown are the *average* temperature for the lower and upper compartments. The maximum temperatures predicted at the end of the transient by CFAST is ~ 540 K for the lower compartment, and ~ 300 K for the upper compartment. The temperature profiles predicted by FDS at the *specific locations* T2.8, and at the human target (1.5 m above the floor at center of upper compartment) are shown in the Figure. The temperature of the hot gas at the human target approaches 366 K at the end of the transient.

Figure 49 shows the pressure development for Case 3. The pressure predicted by FDS at T2.1 becomes negative to ~ -10 Pa as discussed above. The predicted at T2.11 by FDS is initially negative and then becomes positive to ~ 2 Pa at the end of the transient. The lower region of the lower compartments is maintained at a negative pressure through out the transient, but the pressure in the lower region of the upper compartment becomes positive at the end of the transient because the flow into the compartment from the hatches is greater than the flow out from the mechanical vents which is kept constant. Therefore, flow is into the compartment from the side vents in the lower compartment, but out of the compartment from the side vents in the upper compartment toward the end of the transient. The corresponding flows through the side vents is shown in Figure 50. The flow through the lower and upper side vents approach ~ 247 kg/s and -100 kg/s, respectively.

Figure 51 shows the evolution of the surface temperatures in the targets predicted by CFAST. The temperatures for targets B1 and C1 are predicted to reach ~ 556 K and ~ 432 K, respectively, at the end of the transient, while the other targets are predicted to not experience any significant increase in temperature. Figure 52 shows the evolution of the surface temperatures in the targets predicted by FDS. The temperatures for targets B1 and C1 are predicted to reach 636 K and 370 K, respectively, at the end of the transient. The beam surface temperatures do not reach the specified damage temperature, and the cable surface temperatures do not exceed the specified damage temperature for the cable centerline.

Figure 53 and 54 shows the mass flows through the hatches predicted by CFAST and FDS, respectively. The corresponding heat flows through the hatches predicted by FDS is shown in Figure 55. As indicated earlier, the hatches are combined for the CFAST zone model. Figure 46 illustrates again the difficulty of implementing a hatch flow model with selection criteria in

CFAST. The selection criteria which determine the direction of the flows result in discontinuities (shown in figure) that are not realistic. Figure 54 shows that the upward flow predicted through both Hatch 1 and 2 by FDS which levels at ~ 130 kg/s. The heat flows through the hatches predicted by FDS approach ~ 20 MW each, with the heat flow through Hatch 1being slightly higher than that through Hatch 2.

3.4 Validation of Models

The CFAST and FDS fire models used in this benchmark analysis have had limited validation for the types of scenarios examined, specifically for flow through hatches. Cooper's correlation that is used in CFAST for predicting vertical flow in horizontal vents has not been verified or validated [Dey, 2002]. Some comparisons with results from tests conducted at the U.S. Navy's test ship, ex-USS Shadwell, have been made. However, the tests were conducted for a different purpose, other than verifying and validating CFAST, and did not provide all the necessary data to verify and validate the hatch flow submodel. Further verification and validation of the submodel for vertical flow in horizontal vents in CFAST will be beneficial. Although, FDS has been validated (i.e. compared with experimental data) for several experiments conducted in large facilities [Floyd, 2002], it would be beneficial to validate FDS for the specific types of scenarios examined here. Specific parameters that would benefit from comparison with experimental data are pressure in the compartments; and flow through the hatches, side vents in the lower and upper compartments, and roof.

4 General Conclusions and Recommendations

4.1 Capabilities and Limitations

4.1.1 FDS

FDS, including Smokeview, provides a comprehensive tool to examine the phenomena involved in the scenarios. The tools were useful in deriving interesting observations regarding the flow patterns through the hatches and ventilation systems. Such observations of flow and ventilation conditions which affect the thermal environment in a compartment cannot be made intuitively, but can only be determined through such CFD analysis.

The specification of the grid size poses a challenge for FDS calculations. Ideally, a grid of 10 cm is optimal for simulating the large eddies in FDS. However, since some compartment modeled can be quite large, it would have been computationally expensive to use such a fine grid size. Also, FDS adjusts the size of the target which is used in the flow calculations to the minimum grid dimensions specified for the problem, if the target dimension is smaller than the grid size specified. This assumption by the code may affect the flow conditions, and therefore the thermal environment around the targets. At the time the analysis was conducted, Version 3 of FDS [McGrattan, 2002] which includes the capability to use multi-blocking, a term used to describe the use of more than one rectangular mesh in a calculation, was not available. This new version of FDS addresses several of the issues related to grid size.

One assumption inherent in the mixture fraction model is that the combustion process is temperature independent, i.e. the state relations between the mass fraction of each species and mixture fraction is fixed. FDS currently includes some approximate techniques to account for this assumption when the oxygen concentration or temperature is too low to sustain combustion. For scenarios where the fire is under-ventilated, the flame sheet will be extended to regions where the fuel and oxygen are at the ideal stochiometric ratios input to the code. However, this does not indicate the presence of combustion in those regions because the temperatures may not be high enough to sustain combustion.

4.1.2 CFAST

CFAST is computationally efficient, providing the ability to provide solutions to problems within minutes using modern computers. Updating and improving the user interface and documentation will make the code even more efficient.

Modeling horizontal vents in zone models pose several challenges. Firstly, since a zone model is a lumped model for each compartment, it is not possible to represent horizontal vents at different

locations in the compartment. All horizontal vents have to be combined and represented by one vent, or a specific vent needs to be chosen for analysis while ignoring others that may not have an effect on compartment conditions. This may be a significant limitation because there could be important flow phenomena which differ when more than one vertical vent is present.

It should be noted here that others have been successful in using zone models to predict vertical flows through horizontal vents [Rockett, 1992]. The reader is encouraged to review these other techniques for simulating vertical flows through horizontal vents in zone models. Also, this limitation in CFAST may be addressed by conducting bounding calculations of the thermal environment in the compartments.

The interpretation of flows through vents and hatches in CFAST can be complex since it is a zone model and the compartments are divided into an upper and lower layer. Therefore flows are provided for both layers. Although, this is not a fundamental limitation, interpretation of the flows may be difficult when several combinations of flows between the upper and lower layers of different compartments are analyzed.

4.1.3 FDS and CFAST

A detailed heat transfer model for a cable tray will be fairly complex. The CFAST or FDS codes are not capable of modeling complex cable configurations. The CFAST and FDS codes have a simple one-dimensional slab model for targets in which the cable targets are represented as rectangular slabs. A one-dimensional target model may not be adequate since the incident radiative flux would vary with the orientation of the slab. Also, the specification of the slab thickness, and selection of the criterion for cable damage (surface temperature versus centerline temperature) is key to the success of a one-dimensional target model.

4.2 Need for Model Improvements

Both FDS and CFAST could benefit from an improved target model, especially to address the "orientation" issue. However, the benefit from such an improvement will need to be examined given that zone models do not provide local temperatures of the hot gas around the target. There may be a steep vertical temperature gradient in the hot gas, especially for large fires. The fire models include a simple 1-D sub-model for the target that allows the modeling of one cable. This is acceptable as long as the goal of the analysis is to provide a conservative estimate. The modeling of a cable bundled with other cables in a tray will result in lower cable temperatures. The ability to model bundled cables, and the structure of the cable tray, may be beneficial. The ability to model a target with more than one material may also be useful to determine the temperature gradient in the cable. Target heating in the plume and ceiling jet regions will also be beneficial improvements to CFAST.

Previous versions of CFAST have been provided with a GUI to enhance the user interface. The lack of a GUI for CFAST Version 5.0 may lead to errors by users. The GUI for CFAST should be updated and improved to be compatible with more recent versions of Windows. The GUI should provide automatic controls for the input of data and alert the user when values are beyond recommended ranges, or are incorrect. A GUI with this type of feature to check for errors will minimize the input of incorrect data, and the improper use of the model.

4.3 Need for Advanced Models

FDS and CFAST have been useful in analyzing the scenarios specified in the benchmark exercise. FDS, including Smokeview, provides a comprehensive tool to examine the phenomena involved in the scenarios. The tools were useful in deriving interesting observations regarding the flow patterns through the hatches and ventilation systems. Such observations of flow and ventilation conditions which affect the thermal environment in a compartment cannot be made intuitively, but can only be determined through such CFD analysis. CFAST is computationally efficient, providing the ability to provide solutions to problems within minutes.

FDS is useful for verifying the results of CFAST. In this exercise, FDS provided significant insights about the flows through the hatches and limitations of CFAST for modeling vertical flow through horizontal hatches. The FDS model, which is computationally more expensive, may be used to examine the key phenomena in the problem by analyzing a few important scenarios. These results may be used to provide a comparison and verification of the results obtained from FDS.

4.4 Need for Test Programs

The CFAST and FDS fire models used in this benchmark analysis have had limited validation for the types of scenarios examined, specifically for flow through hatches. Further verification and validation of the submodel for vertical flow through horizontal vents in CFAST. Although, FDS has been validated (i.e. compared with experimental data) for several experiments conducted in large facilities, it would be beneficial to validate FDS for the specific types of scenarios examined here. Further verification and validation of the submodel for vertical flow through horizontal vents in FDS will also be beneficial. It is recognized that this is an extremely difficult problem to calculate and measure. Tests are needed to provide data for the validation of both codes to add confidence in their use for regulatory applications.

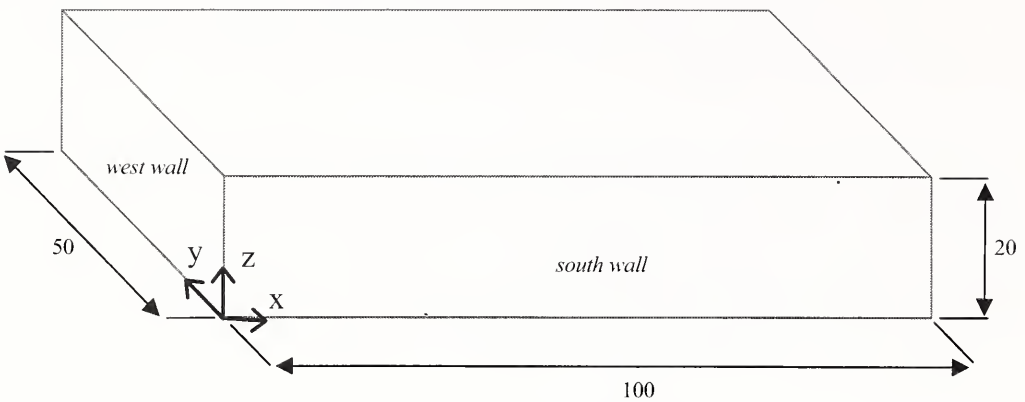

Figure 1 External Dimensions of Hall

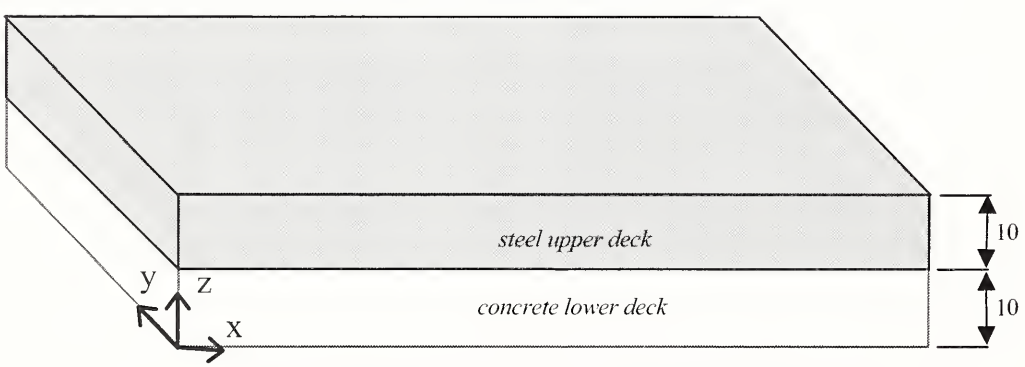

Figure 2 Upper and Lower Compartments

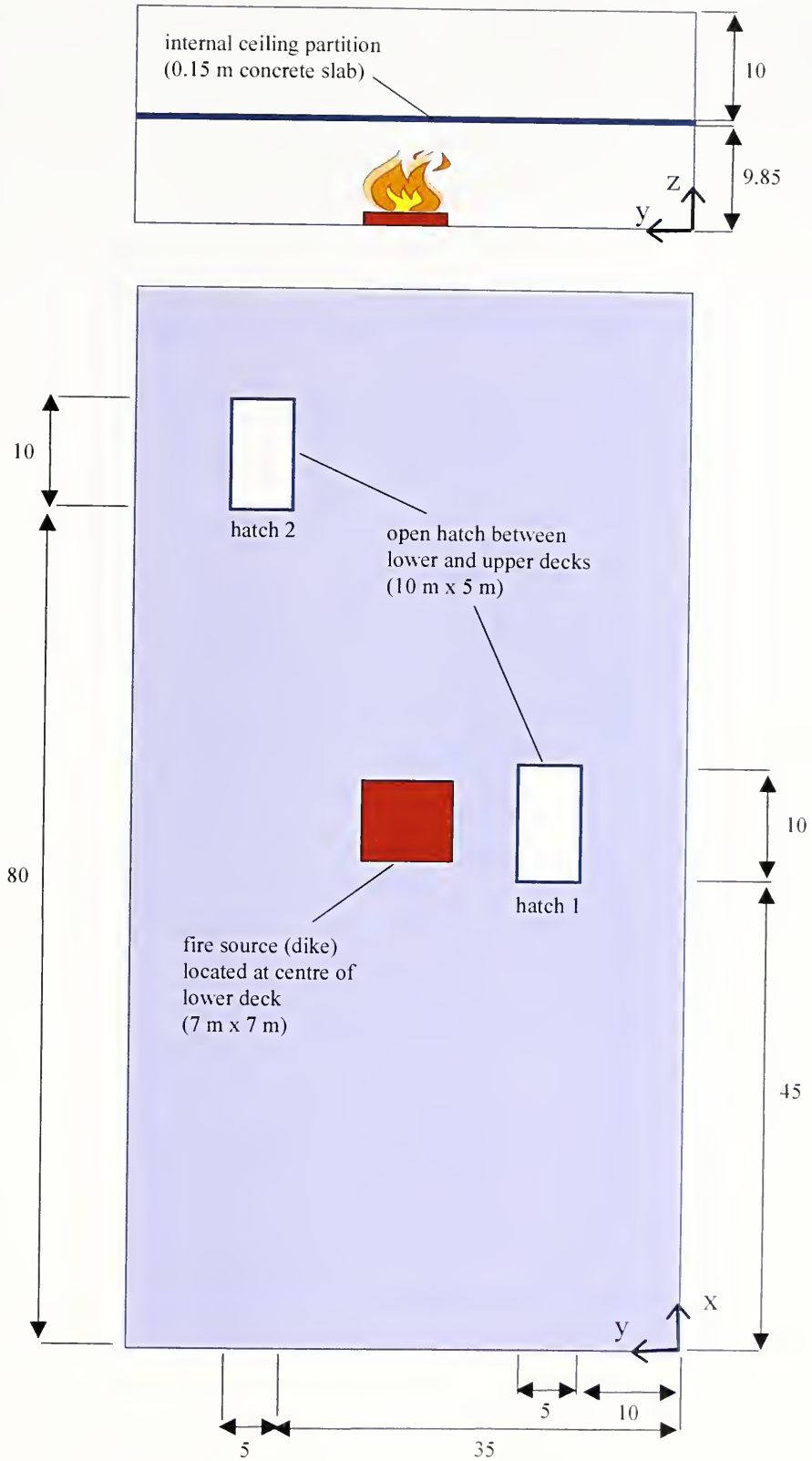

Figure 3 Internal Dimensions of Compartments

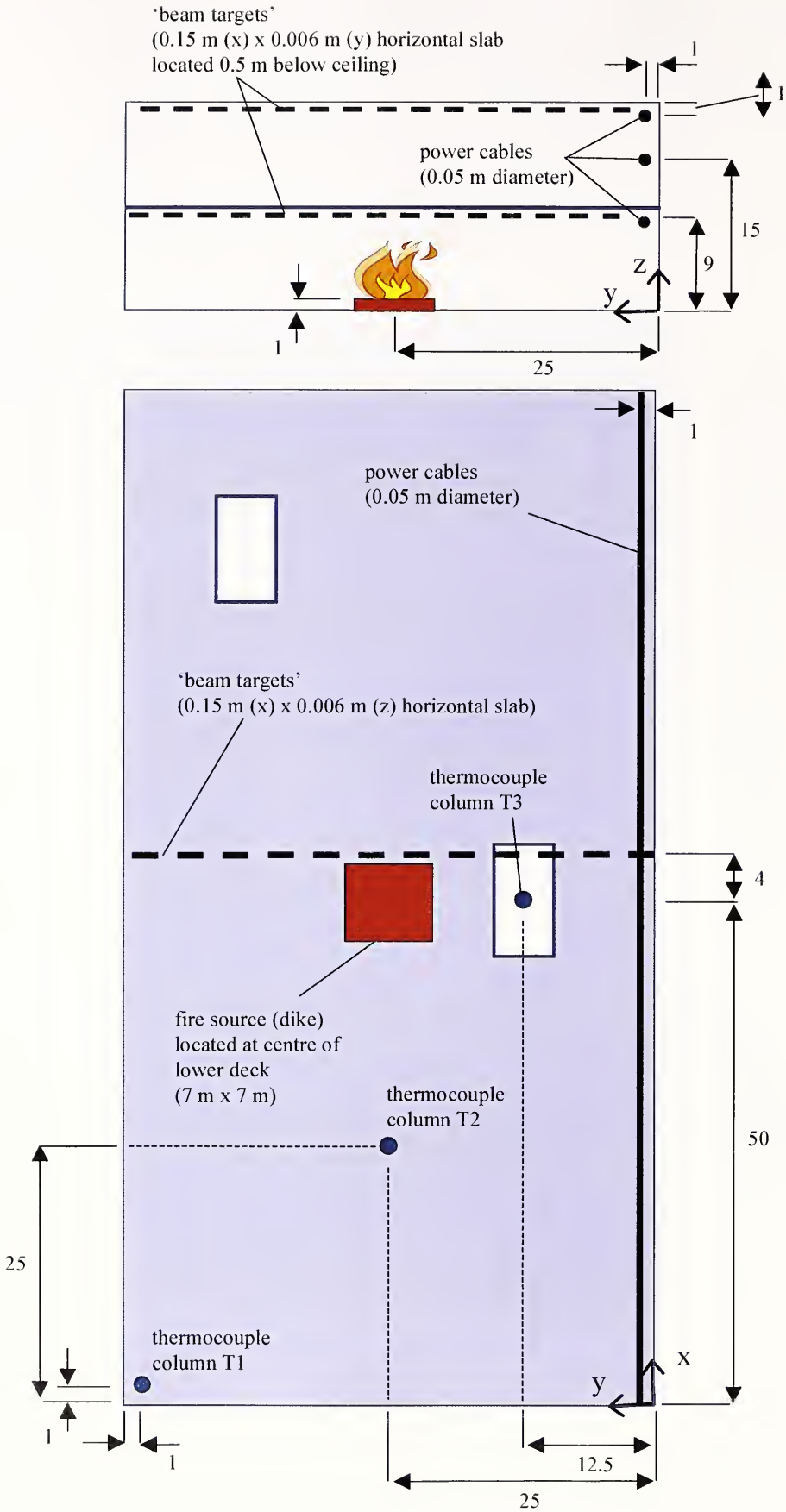

Figure 4 Locations of Thermocouple Trees and Targets

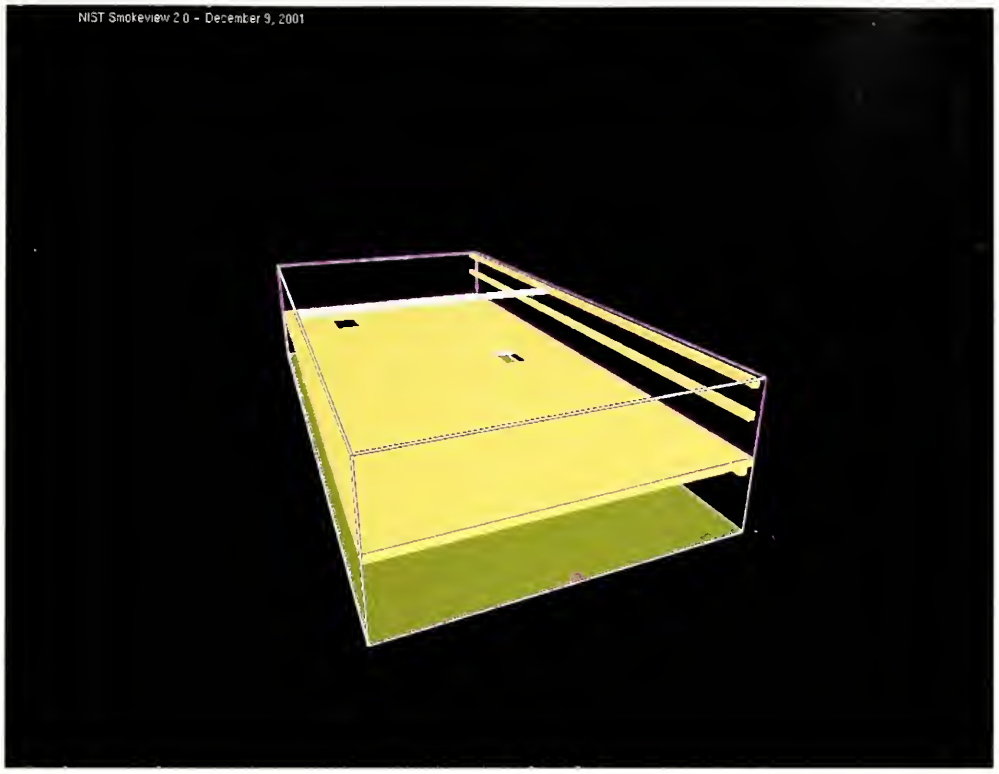

Figure 5 FDS Compartment Model - Case 1

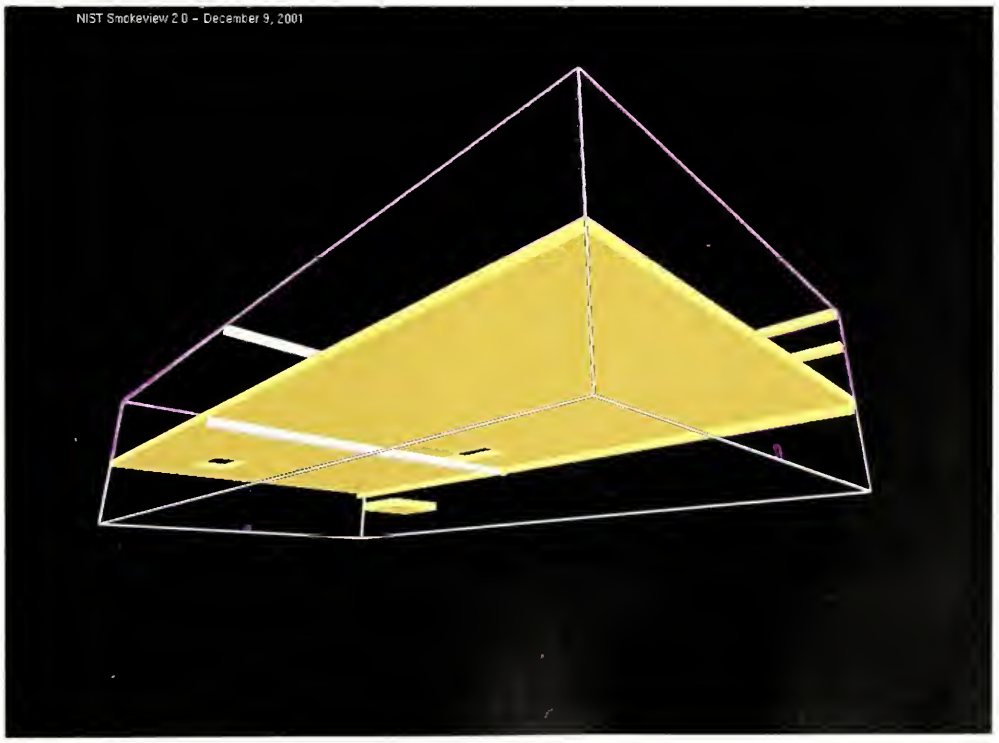

Figure 6 FDS Compartment Model - Case 1

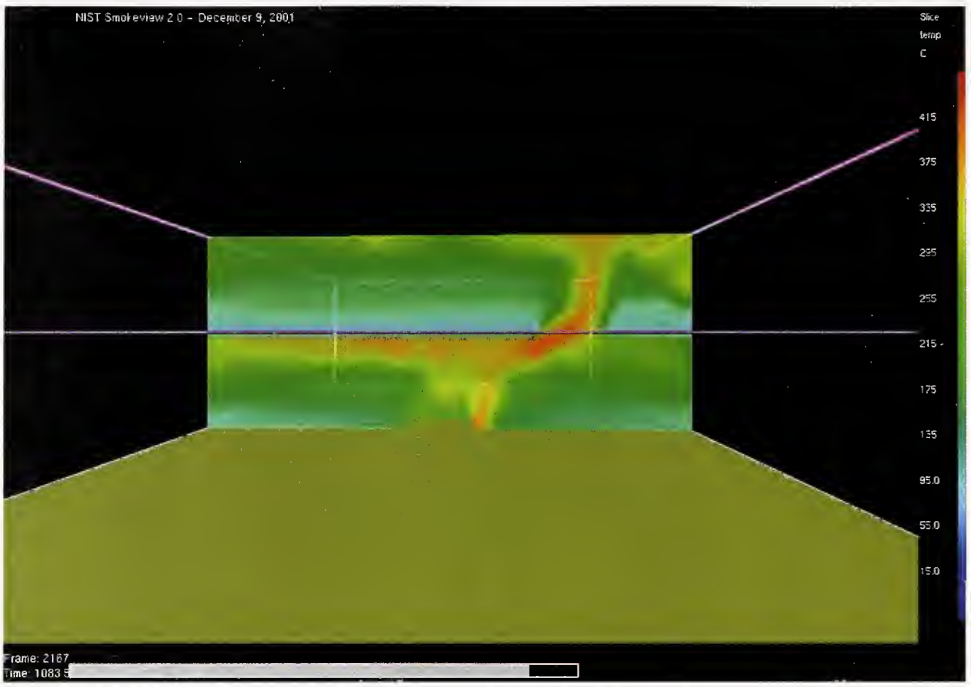

Figure 7 Temperature Profile (1083 s) - Case 1

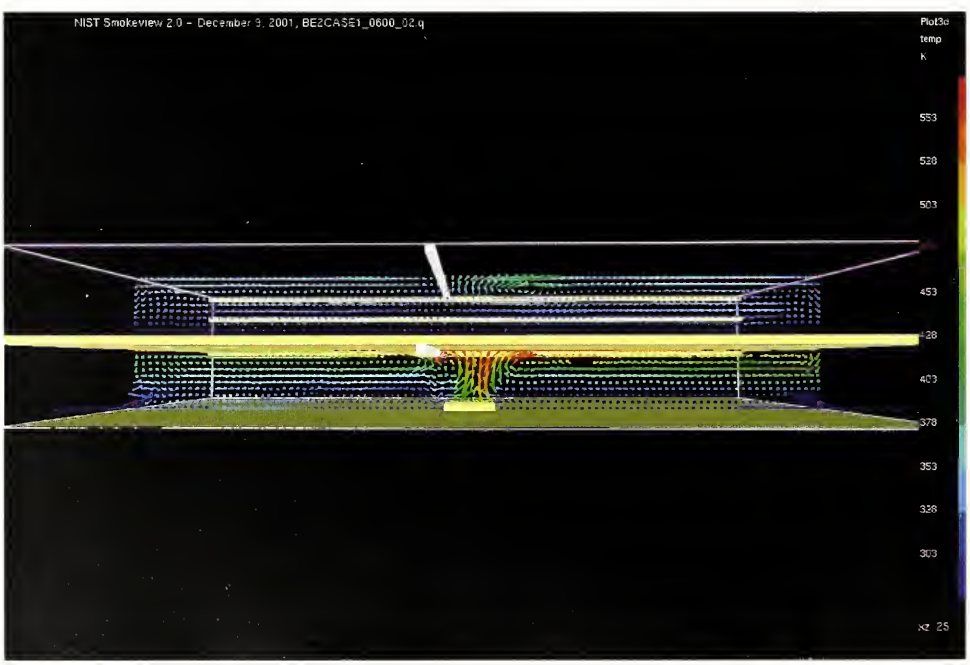

Figure 8 Flow Vectors at Fire & Vents (600 s) - Case 1

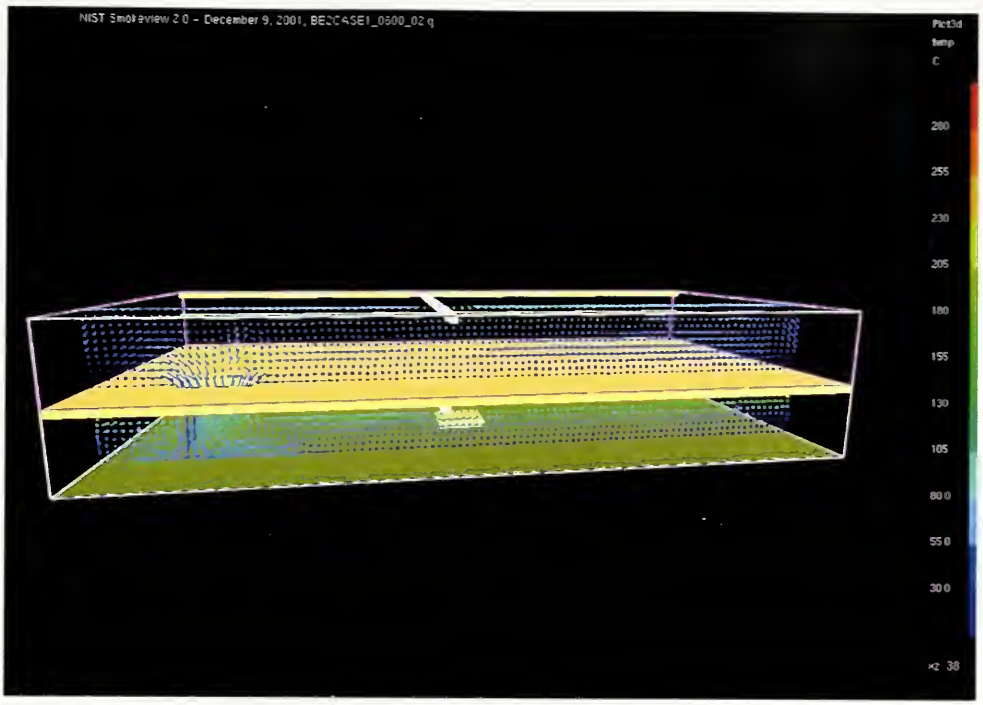

Figure 9 Flow Vectors at Hatch 2 (600 s) - Case 1

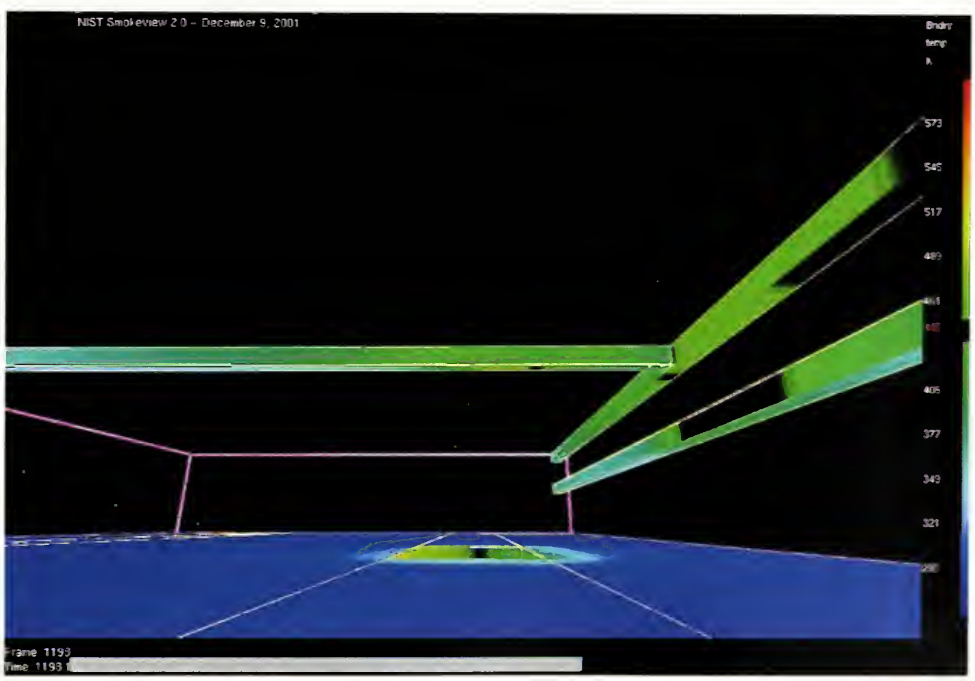

Figure 10 Target Surface Temperatures (1200 s) - Case 1

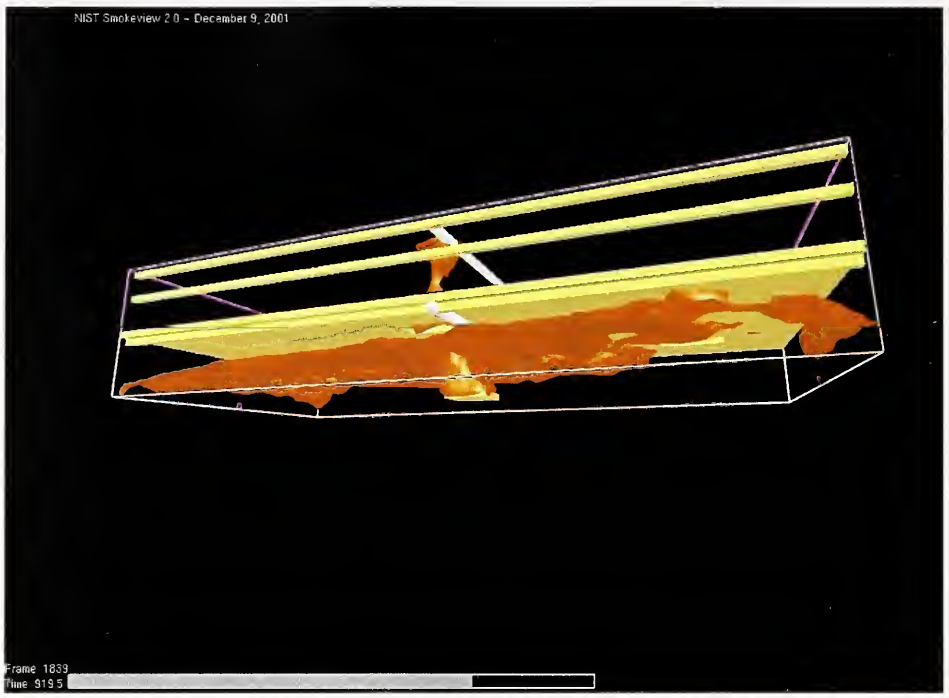

Figure 11 Isosurface of Mixture Fraction = 0.05 (920 s) - Case 1

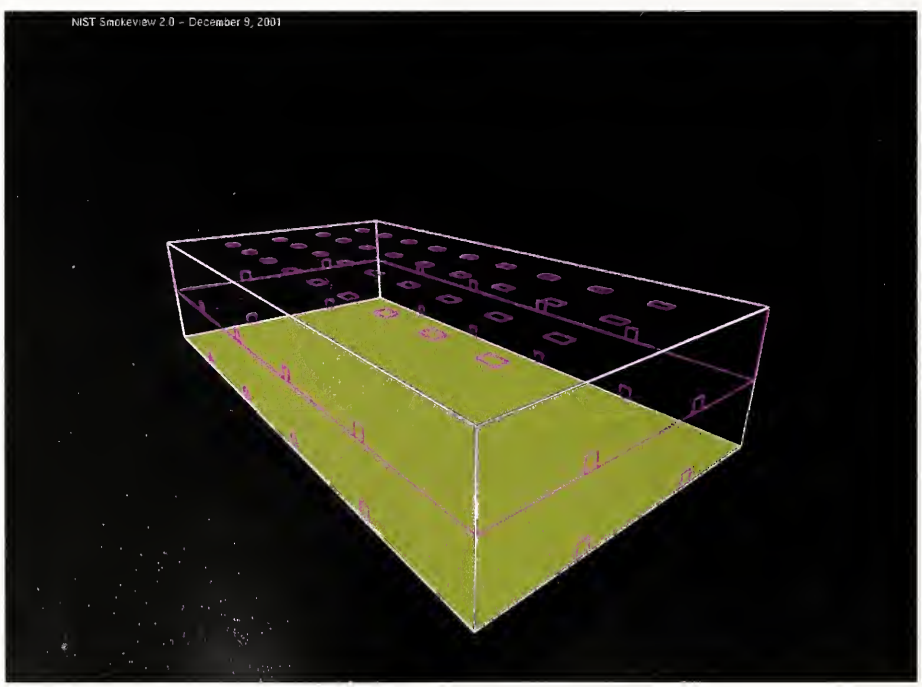

Figure 12 FDS Compartment Model - Case 2

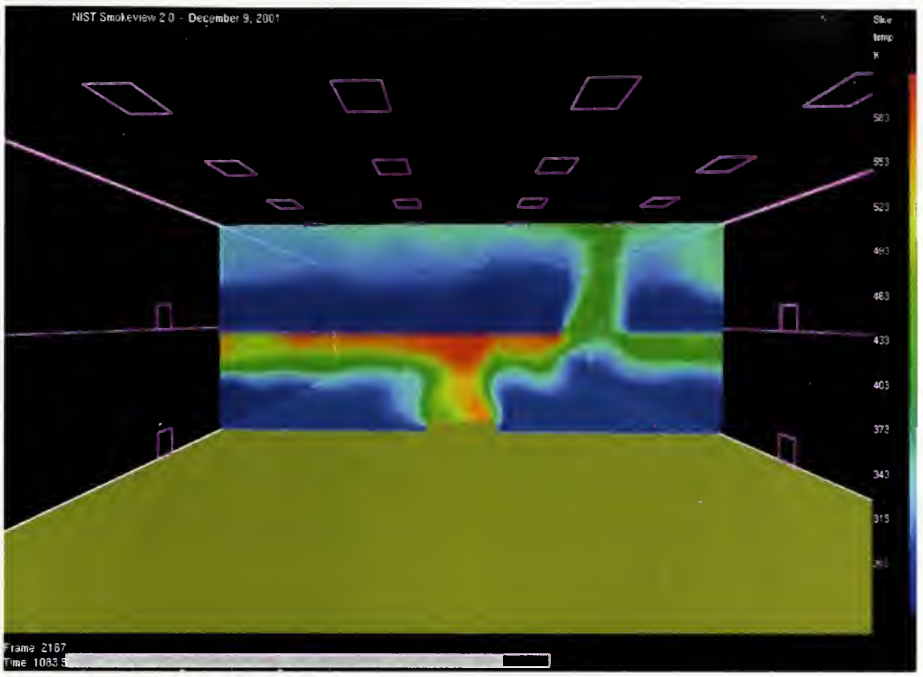

Figure 13 Temperature Profile (1083 s) - Case 2

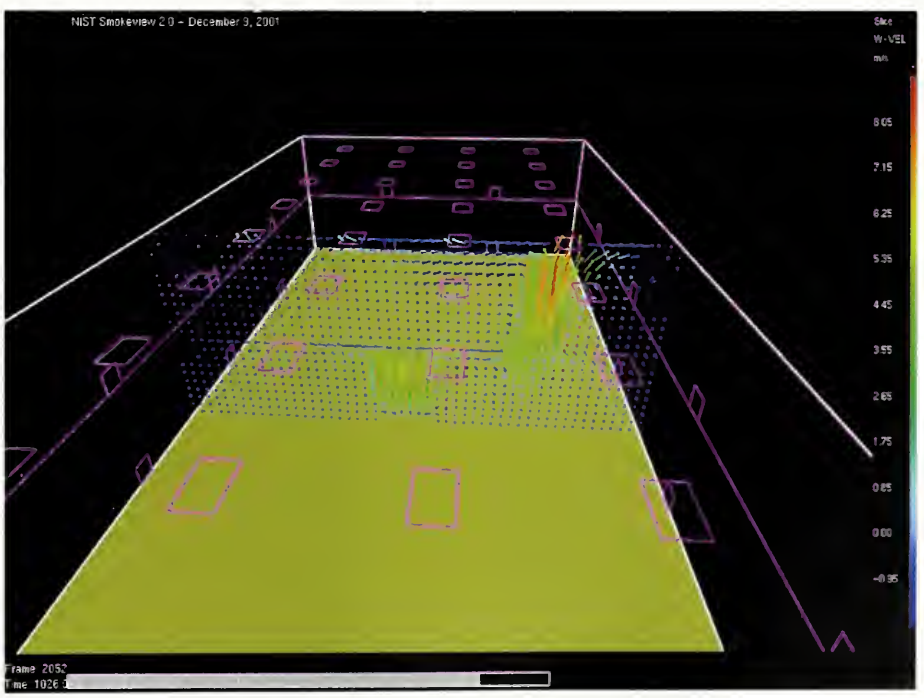

Figure 14 Flow Vectors at Fire, Hatch 1, & Roof Vents (1026 s) - Case 2

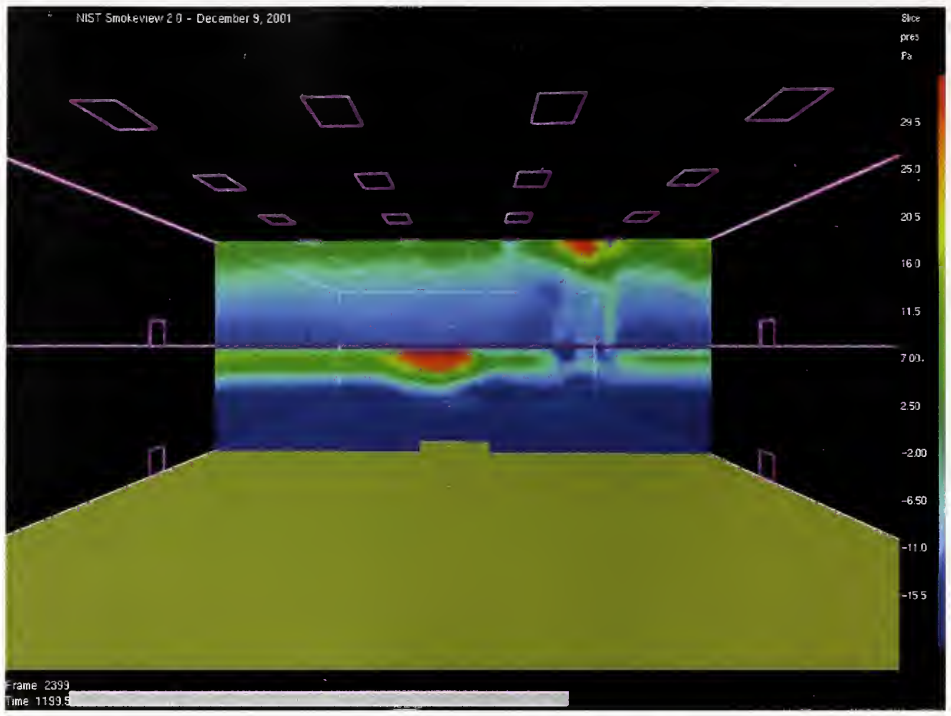

Figure 15 Pressure Profile (1200 s) - Case 2

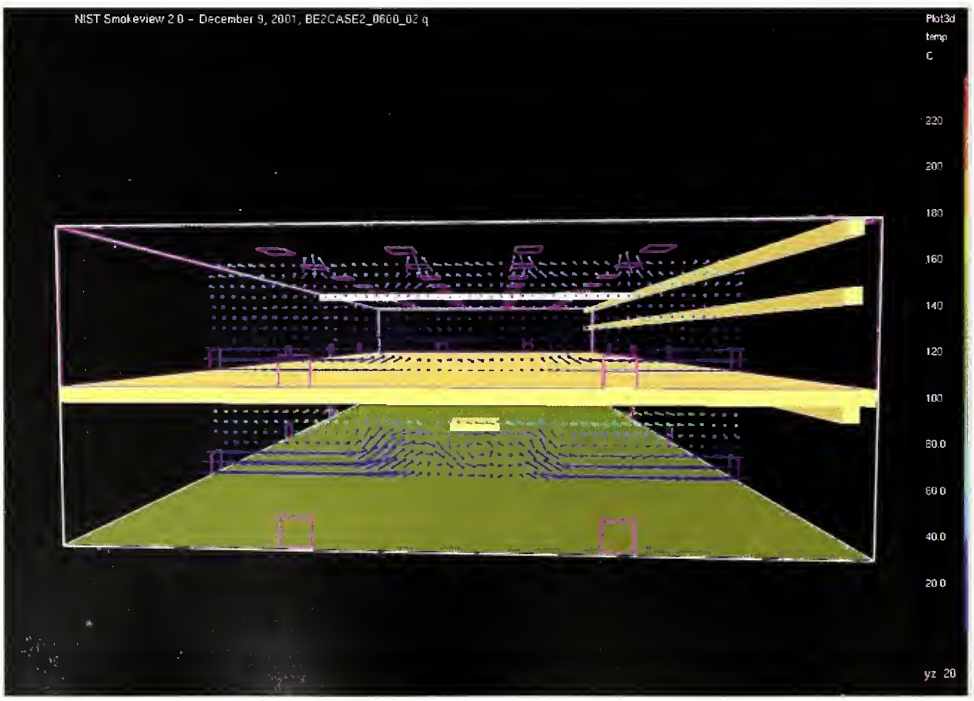

Figure 16 Flow Vectors at Side & Roof Vents (600 s) - Case 2

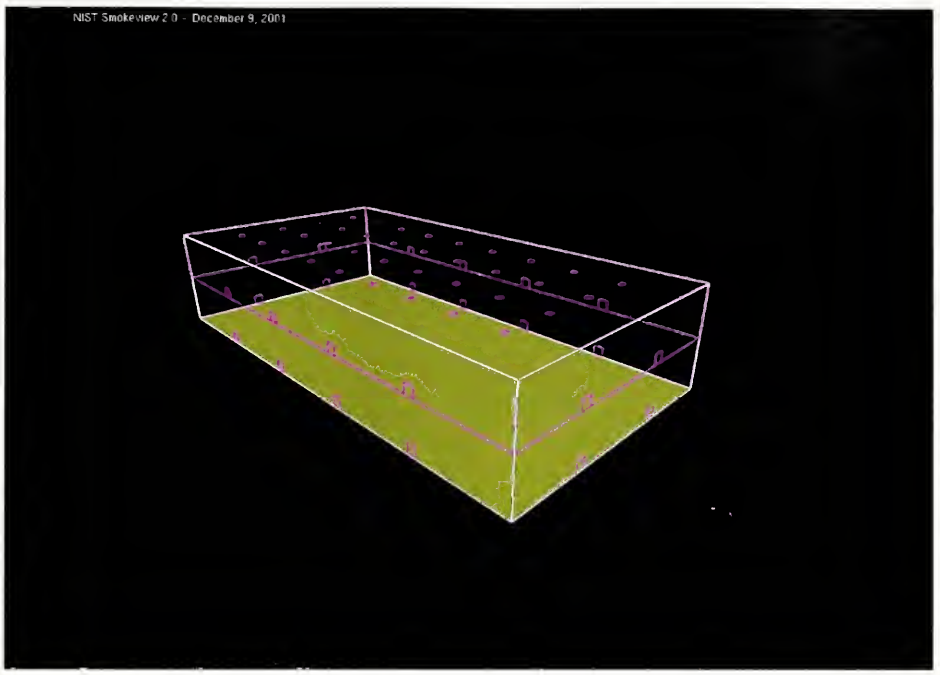

Figure 17 FDS Compartment Model - Case 3

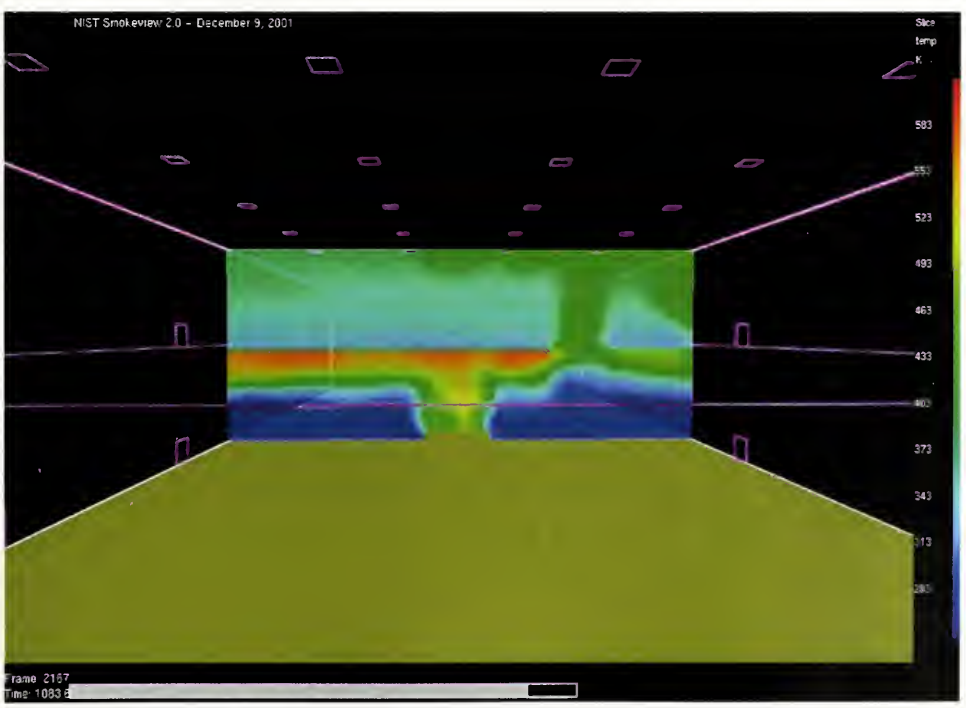

Figure 18 Temperature Profile (1083 s) - Case 3

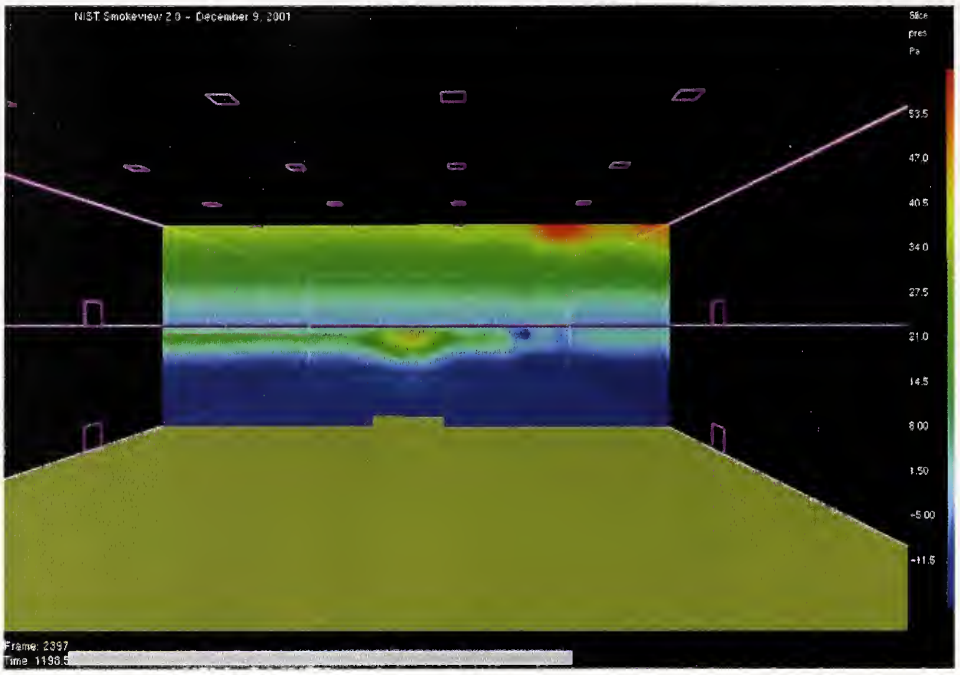

Figure 19 Pressure Profile (1200 s) - Case 3

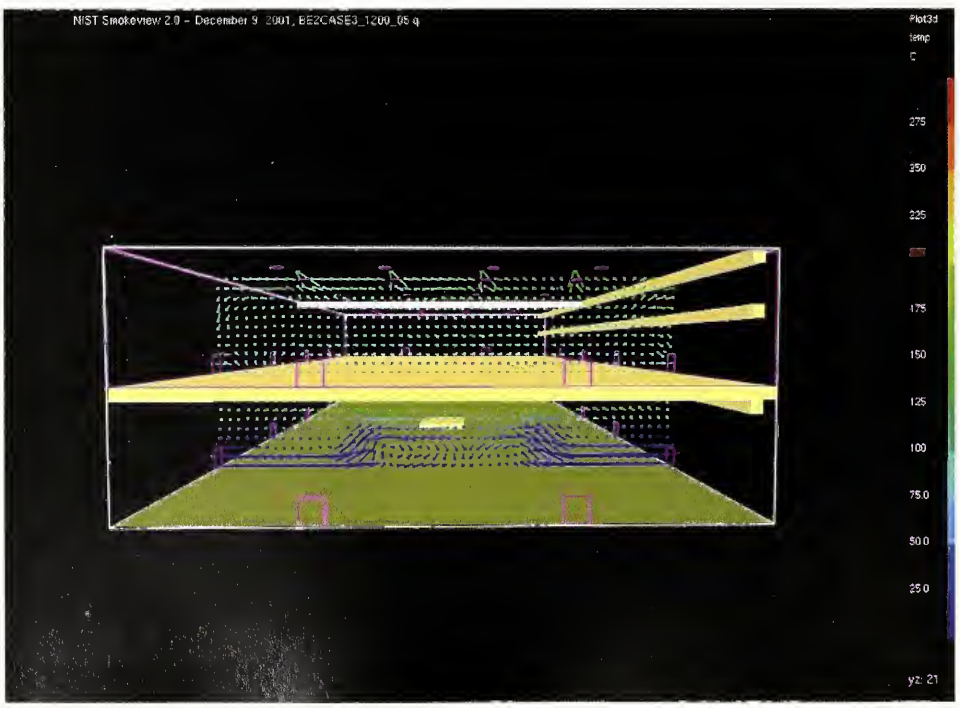

Figure 20 Flow Vectors at Side & Roof Vents (1200 s) - Case 3

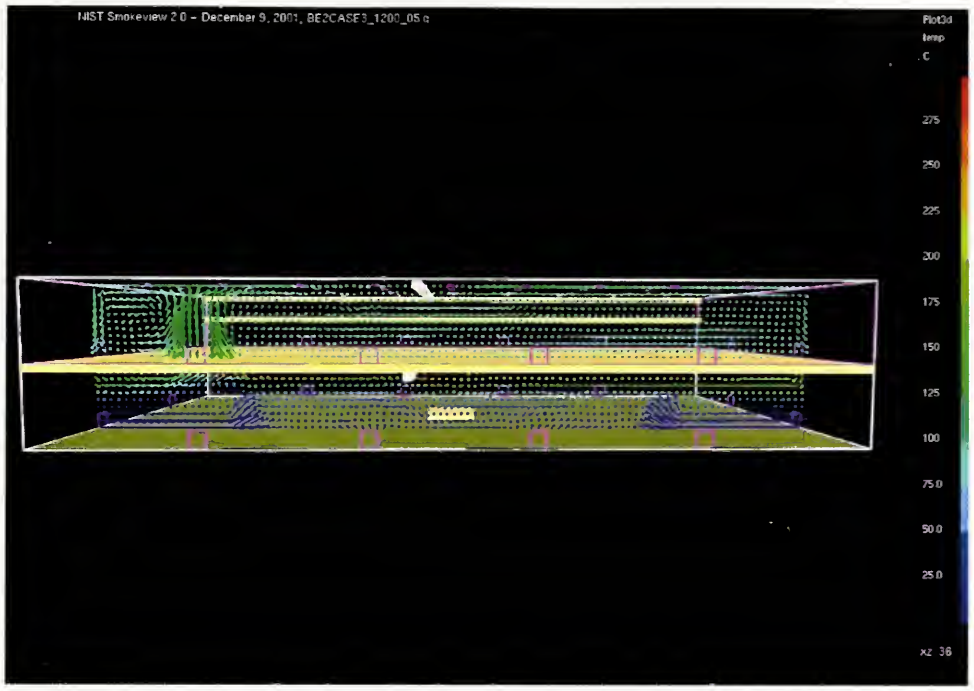

Figure 21 Flow Vectors at Hatch 2 (1200 s) - Case 3

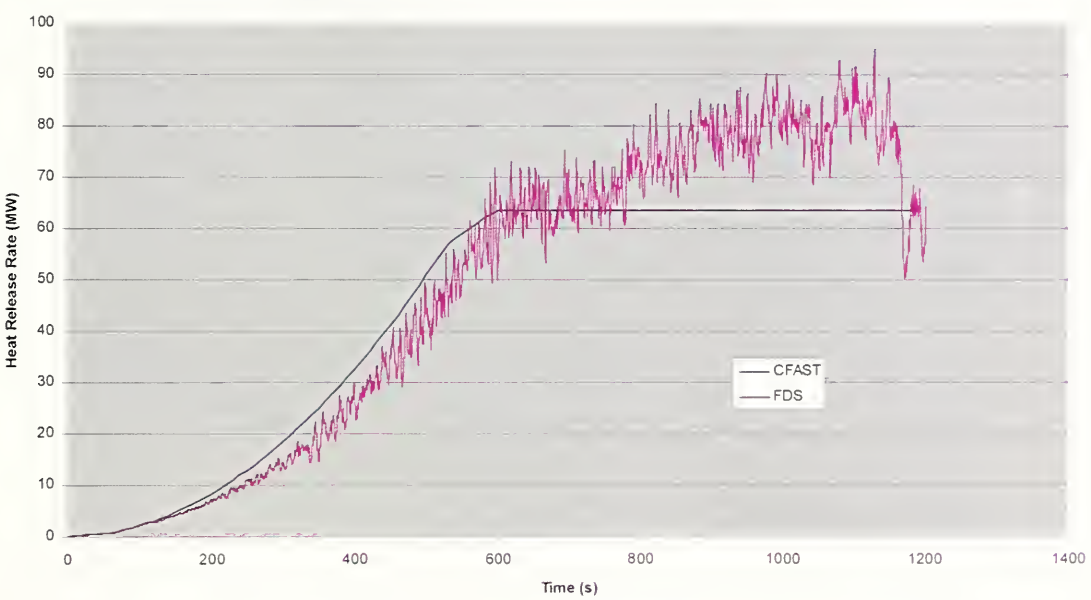

Figure 22 Large Pool Fire - Case 1

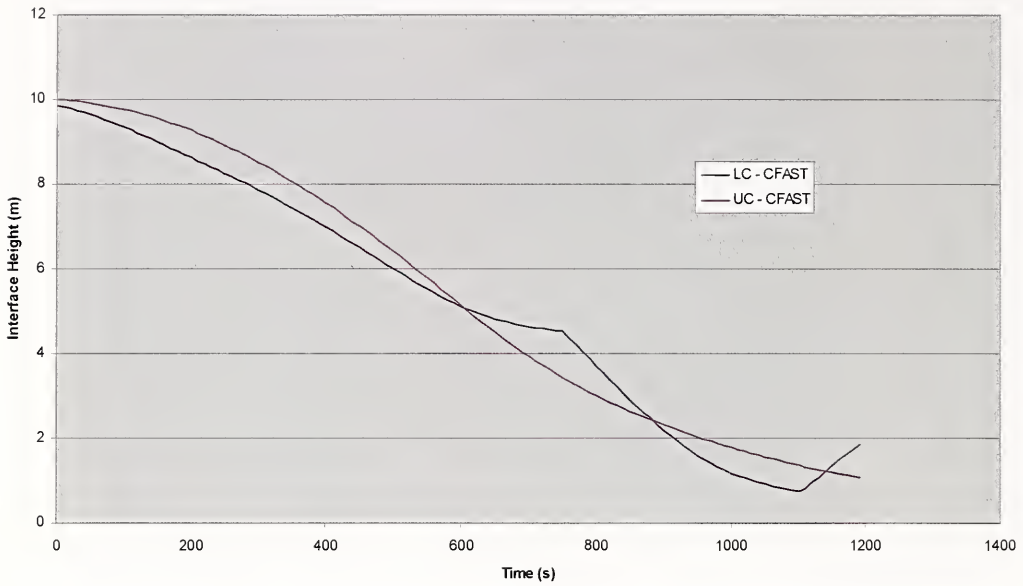

Figure 23 HGL Development - Case 1

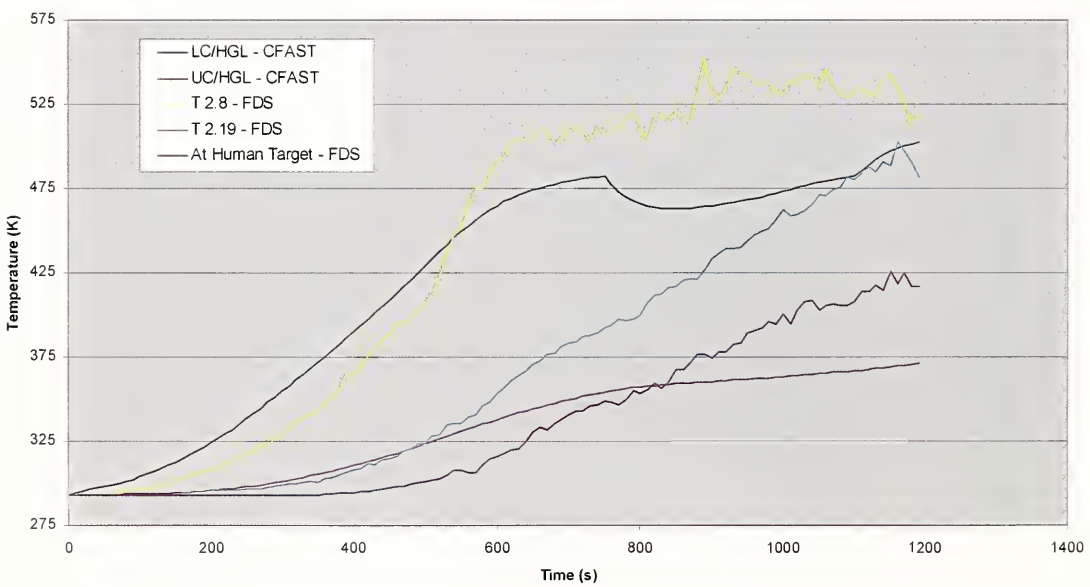

Figure 24 Gas Temperatures - Case 1

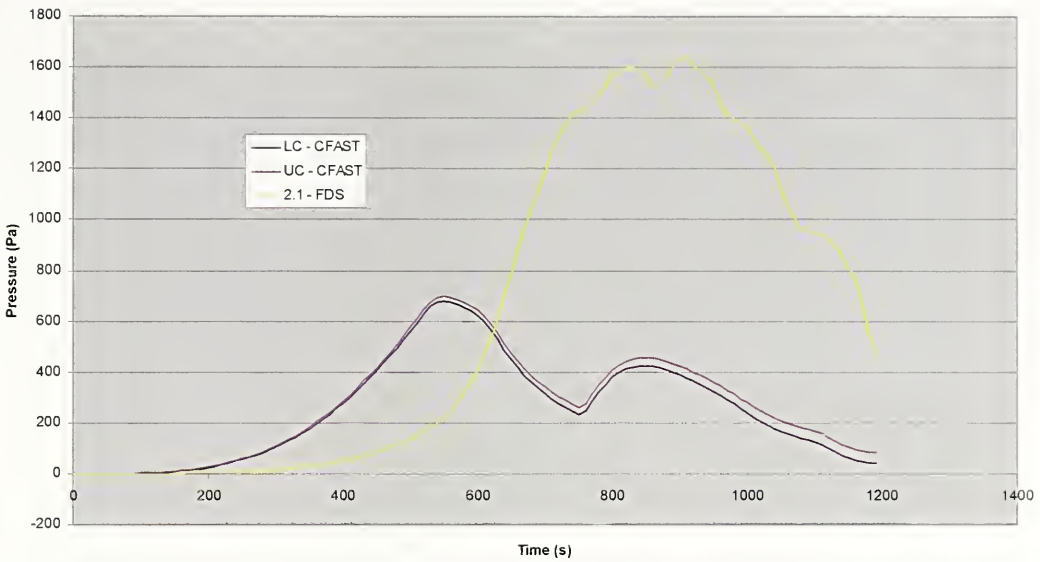

Figure 25 Pressure Development - Case 1

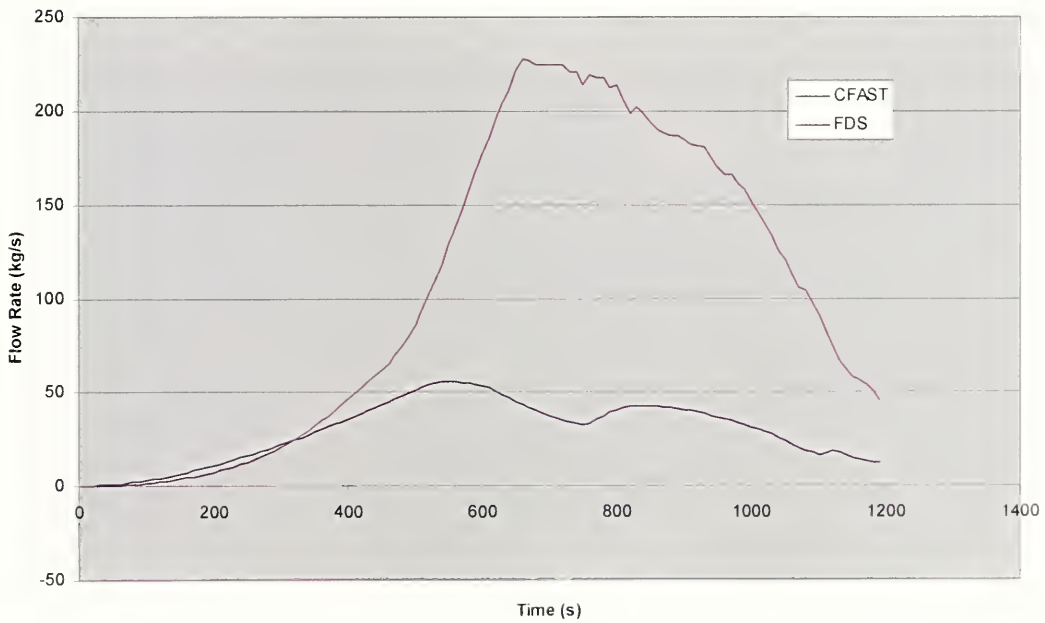

Figure 26 Leak Vent Flow - Case 1

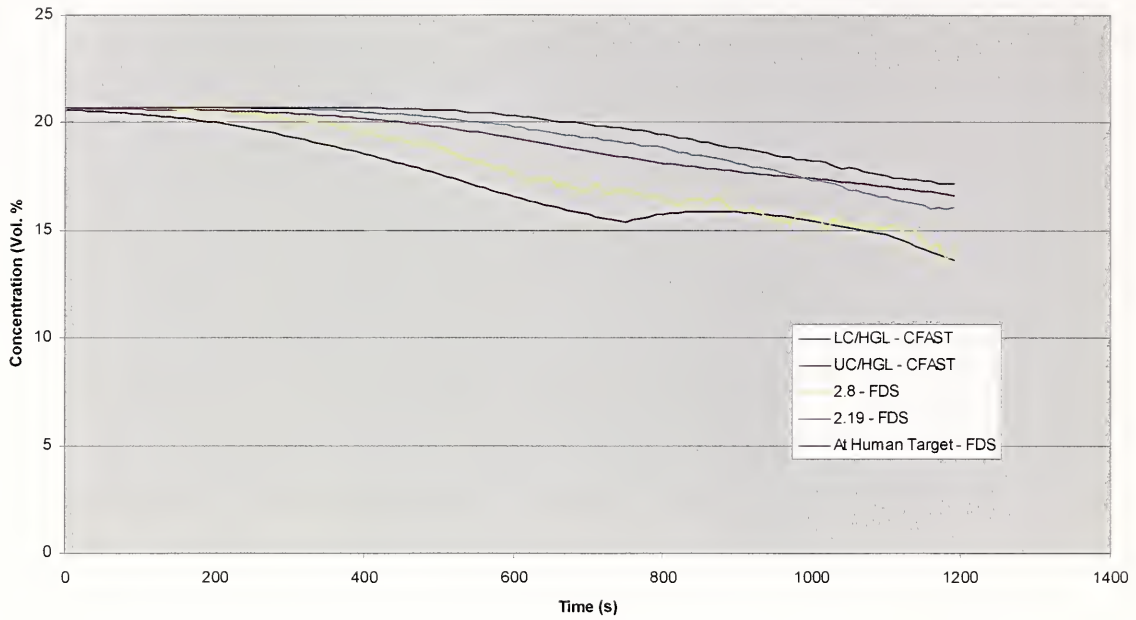

Figure 27 Oxygen Concentration - Case 1

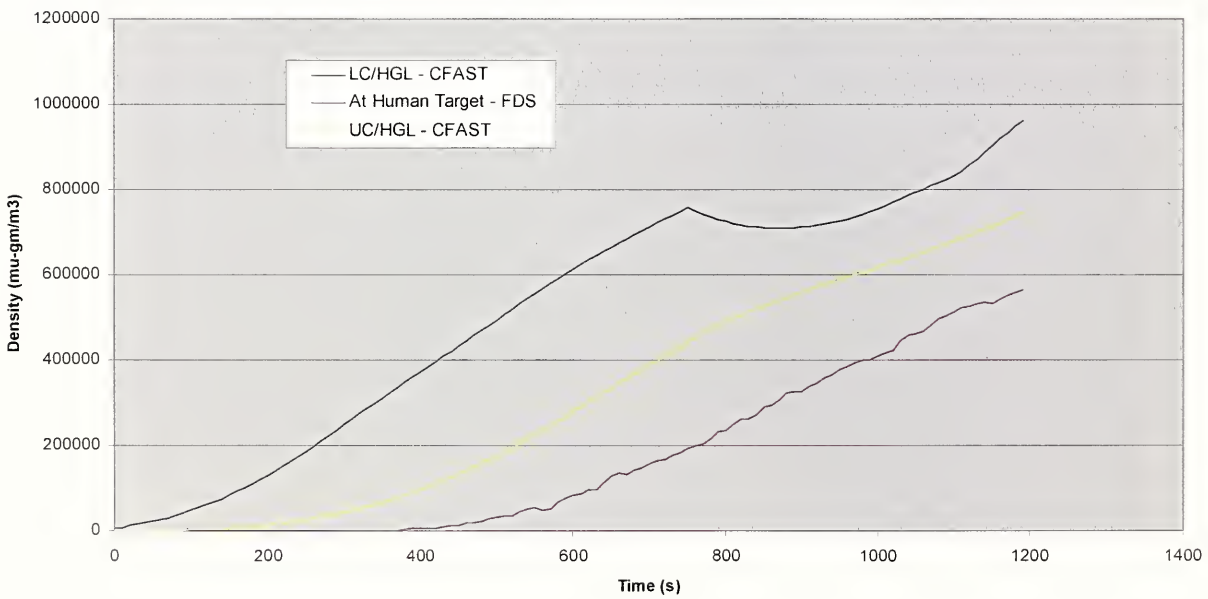

Figure 28 Soot Development - Case 1

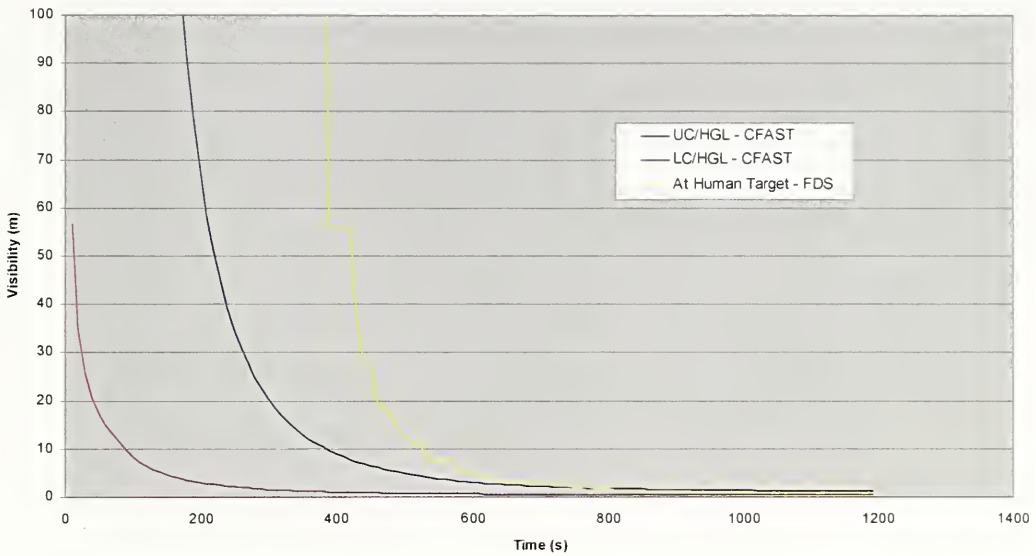

Figure 29 Visibility for Light-Reflecting Sign - Case 1

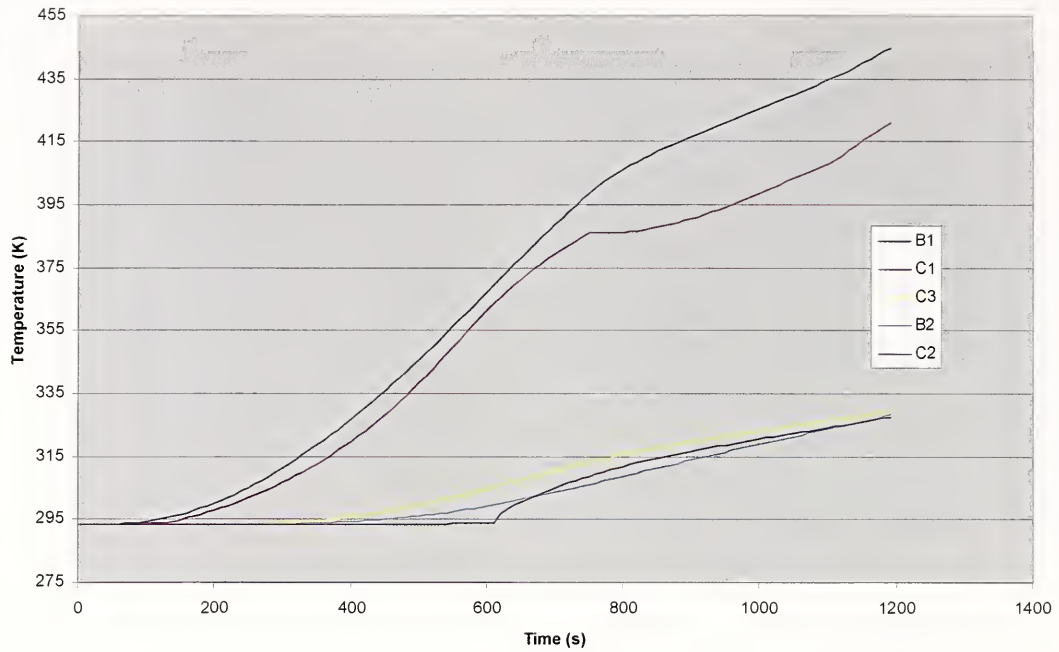

Figure 30 Target Surface Temperatures (CFAST) - Case 1

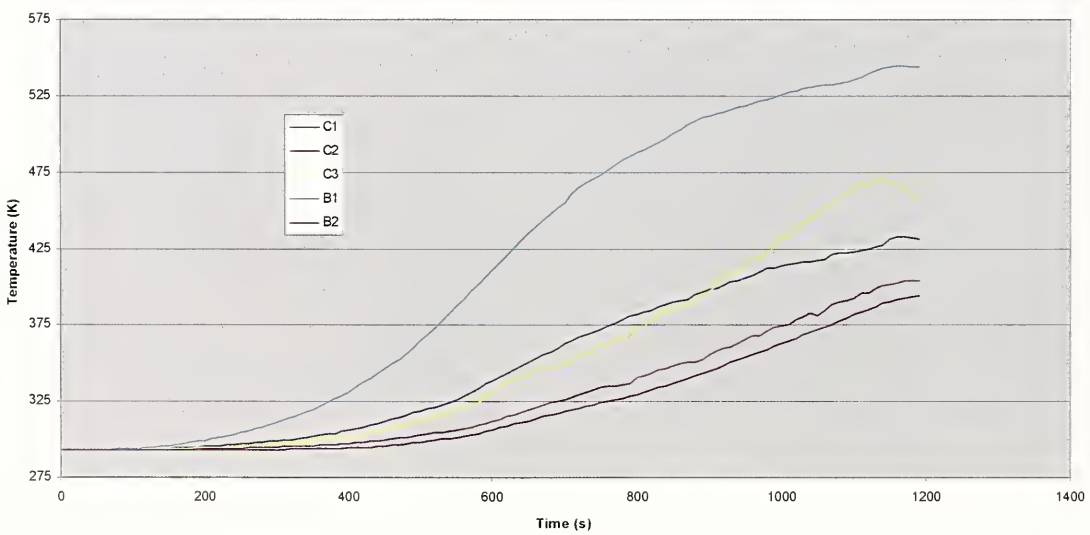

Figure 31 Target Surface Temperatures (FDS) - Case 1

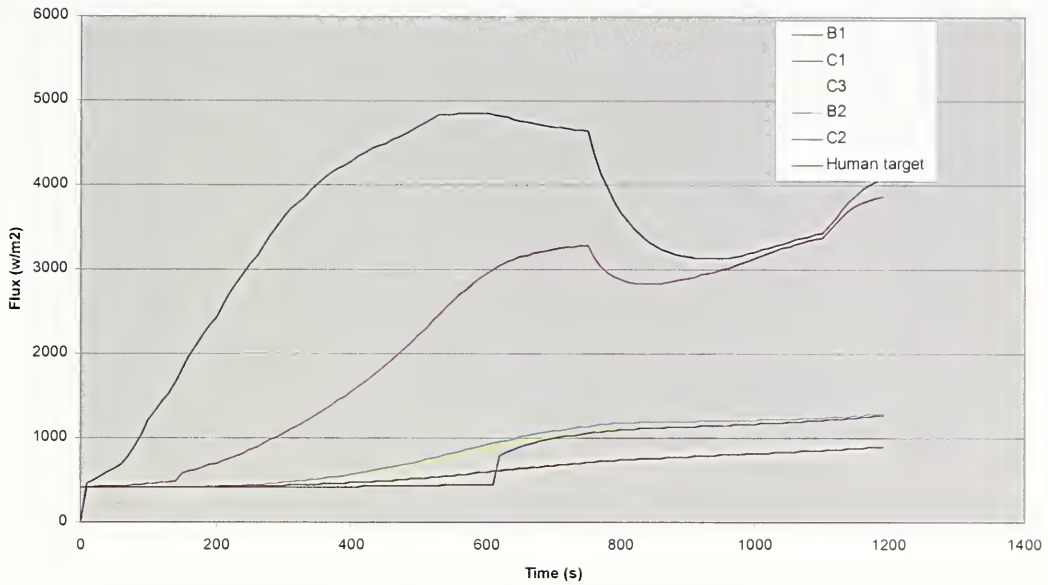

Figure 32 Target Total Flux (CFAST) - Case 1

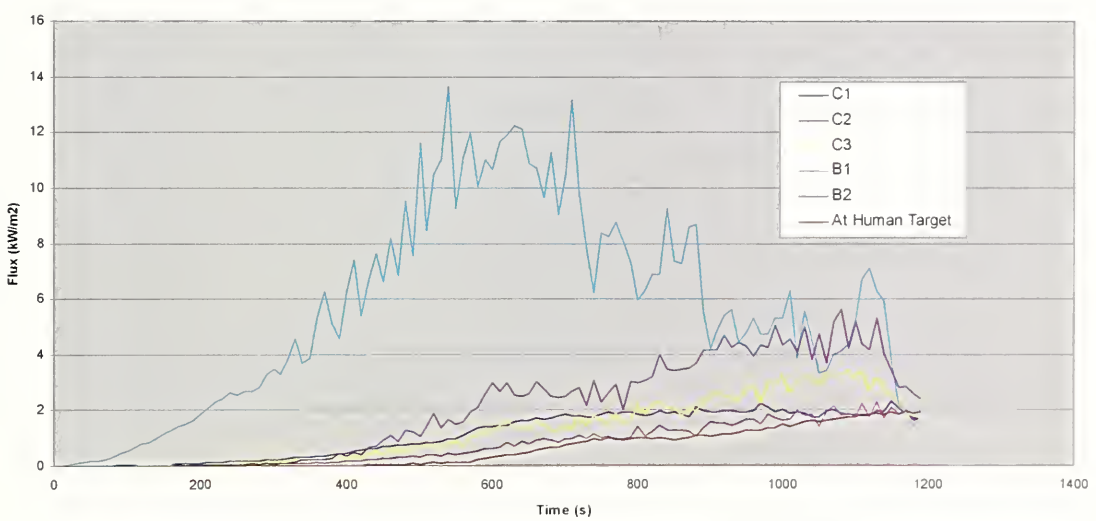

Figure 33 Target Total Flux (FDS) - Case 1

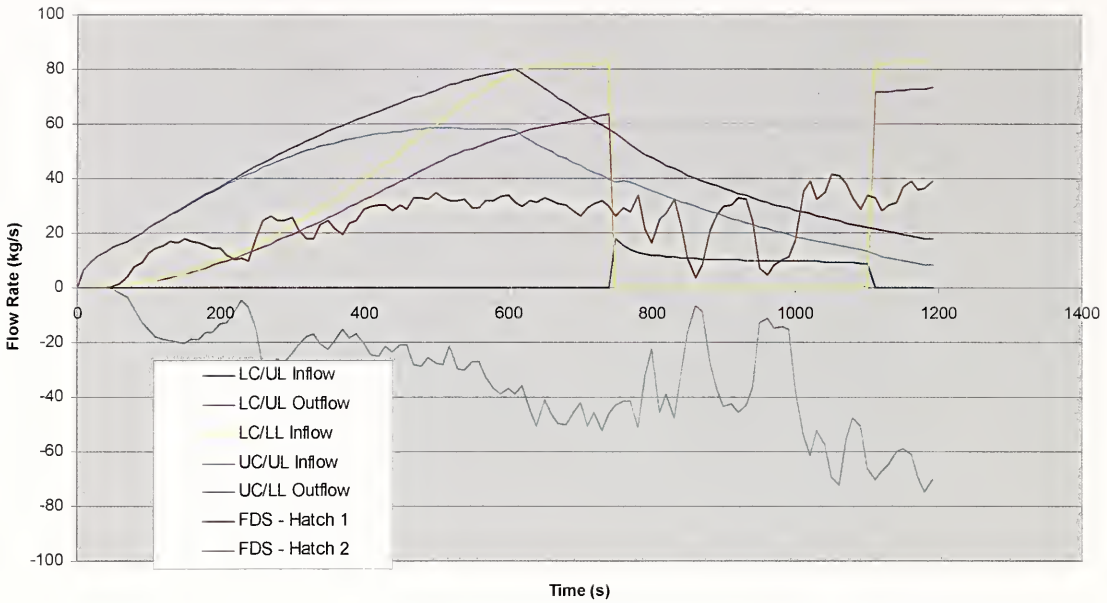

Figure 34 Hatch Mass Flows - Case 1

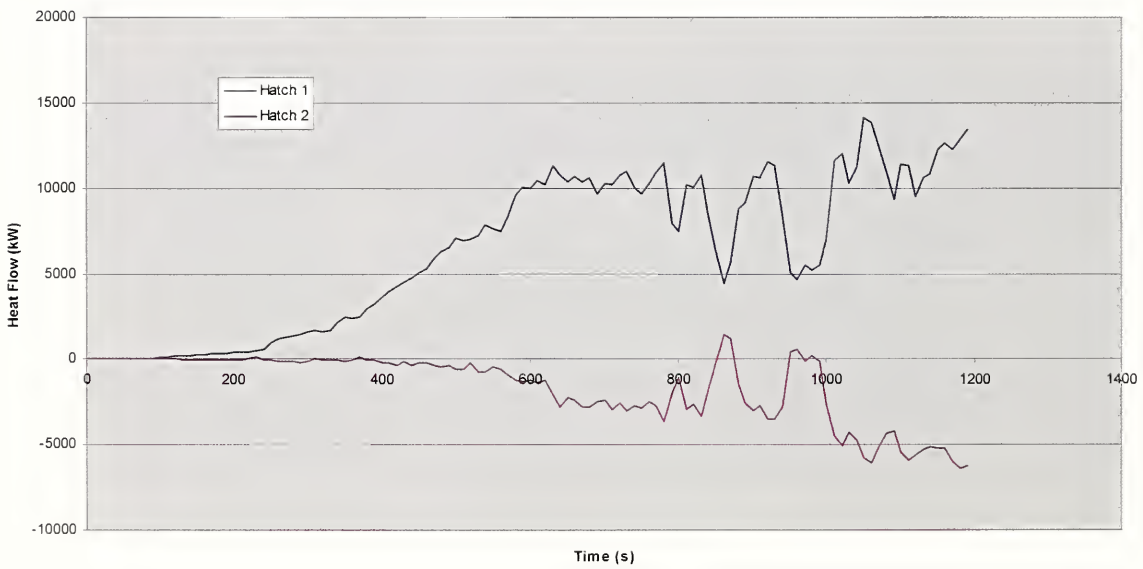

Figure 35 Hatch Heat Flows (FDS) - Case 1

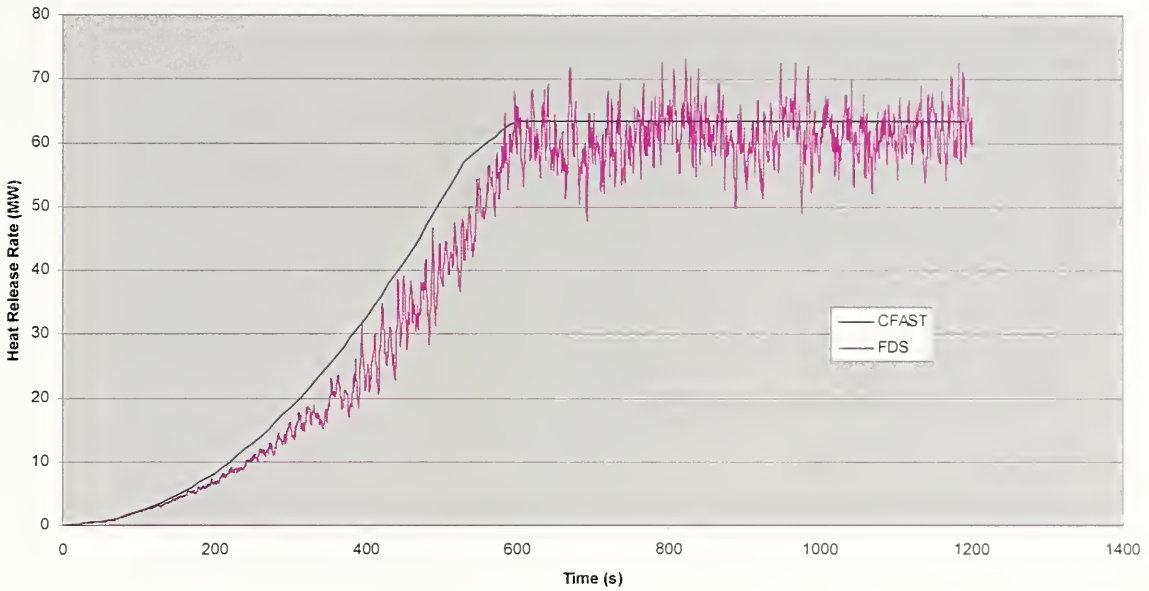

Figure 36 Large Pool Fire - Case 2

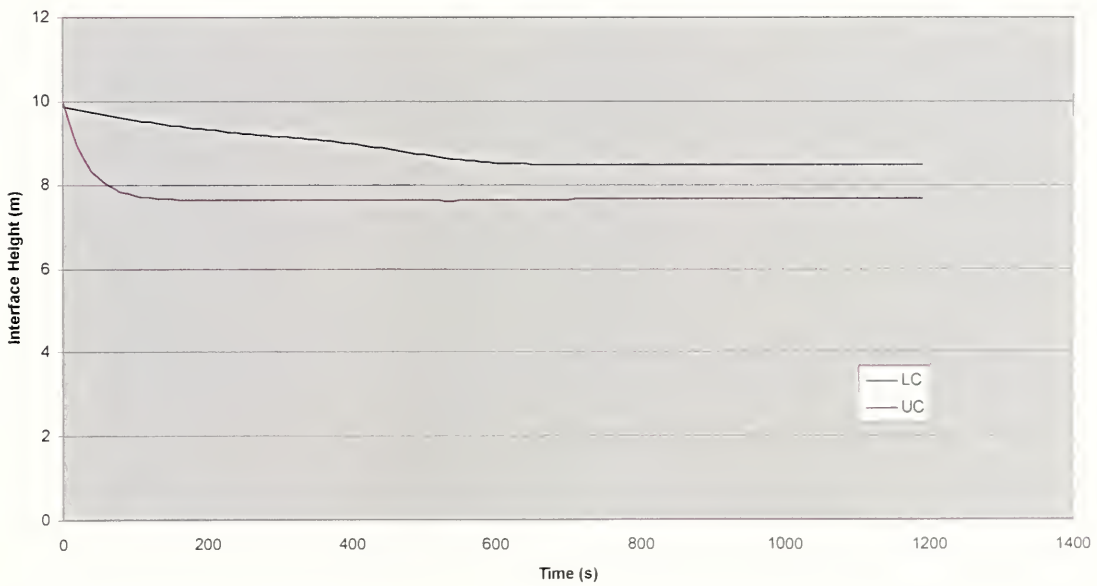

Figure 37 HGL Development (CFAST) - Case 2

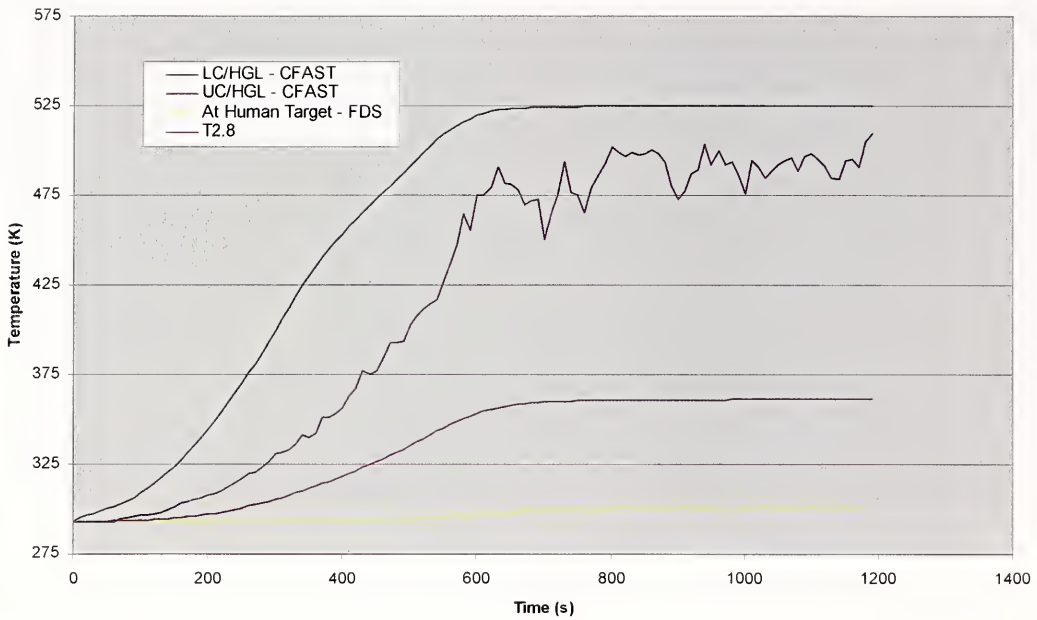

Figure 38 Gas Temperatures - Case 2

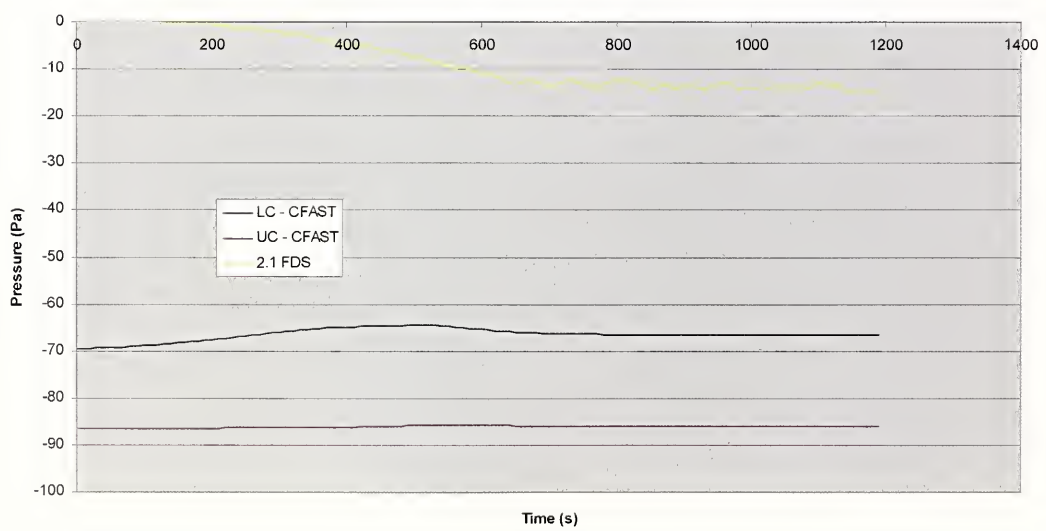

Figure 39 Pressure Development - Case 2

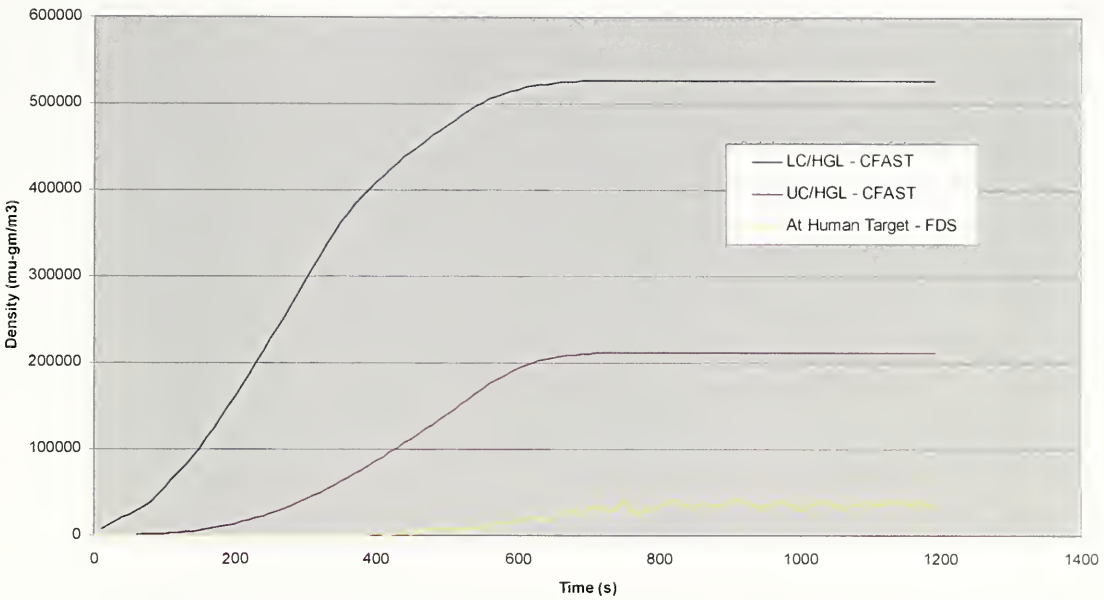

Figure 40 Soot Development - Case 2

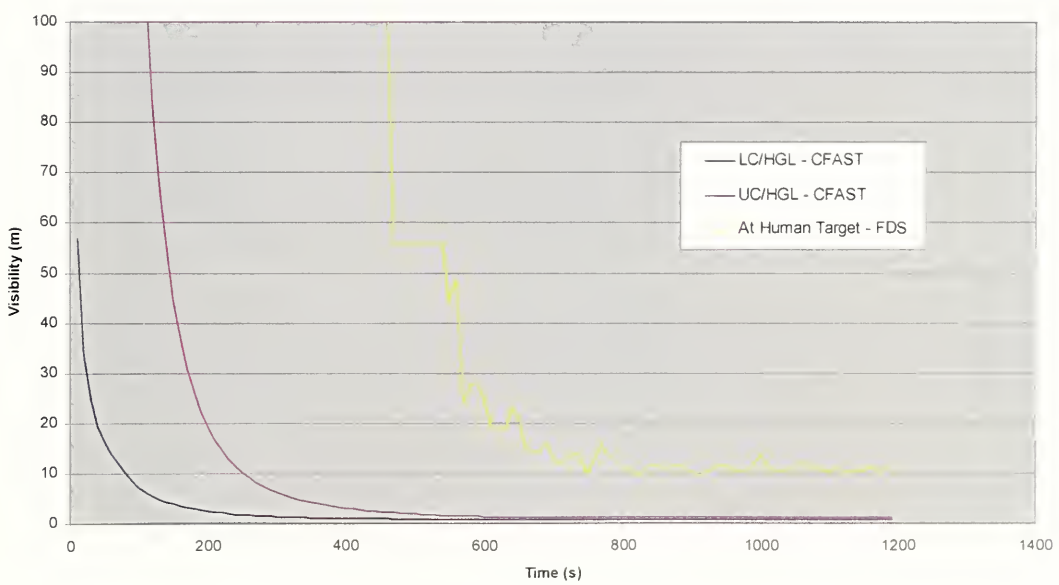

Figure 41 Visibility for Light-Reflecting Sign - Case 2

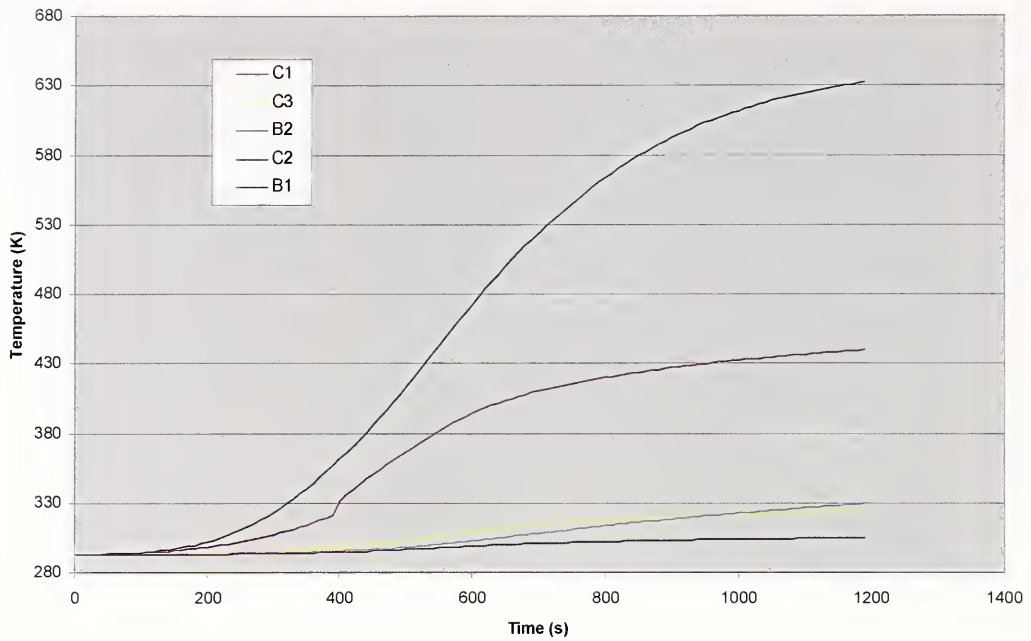

Figure 42 Target Surface Temperatures (CFAST) - Case 2

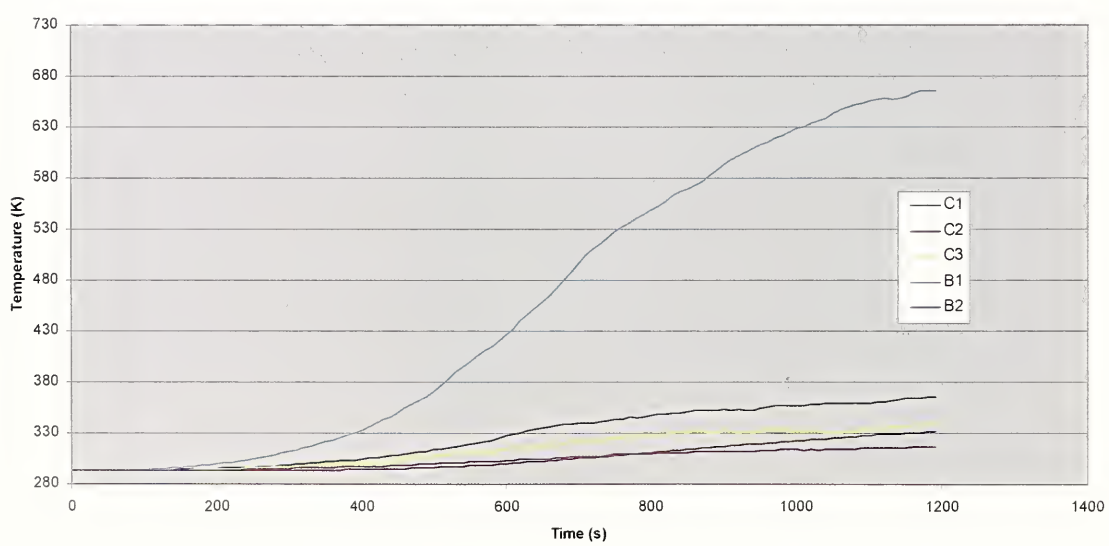

Figure 43 Target Surface Temperature (FDS) - Case 2

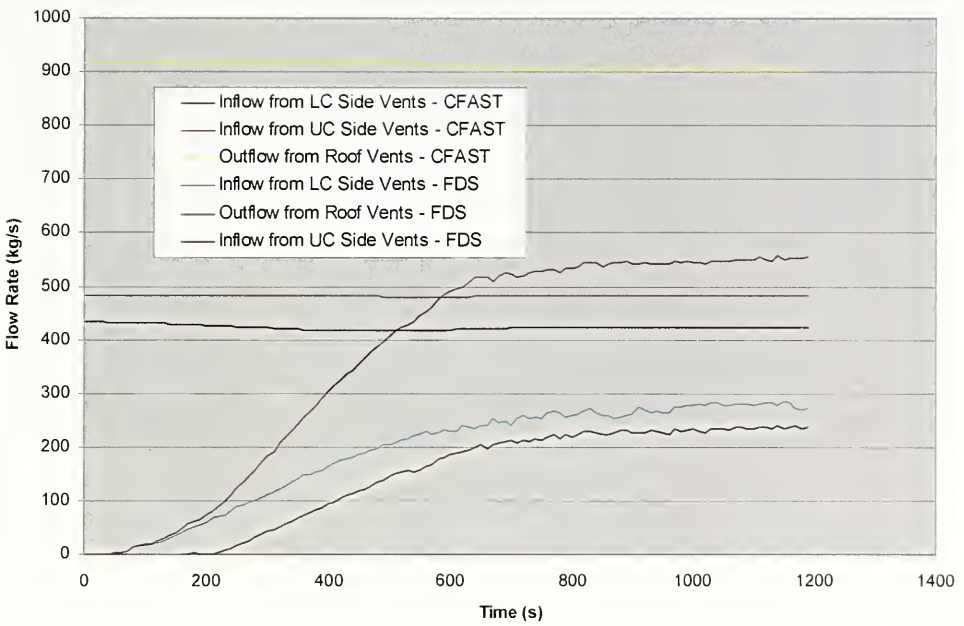

Figure 44 Compartment Vent Flows - Case 2

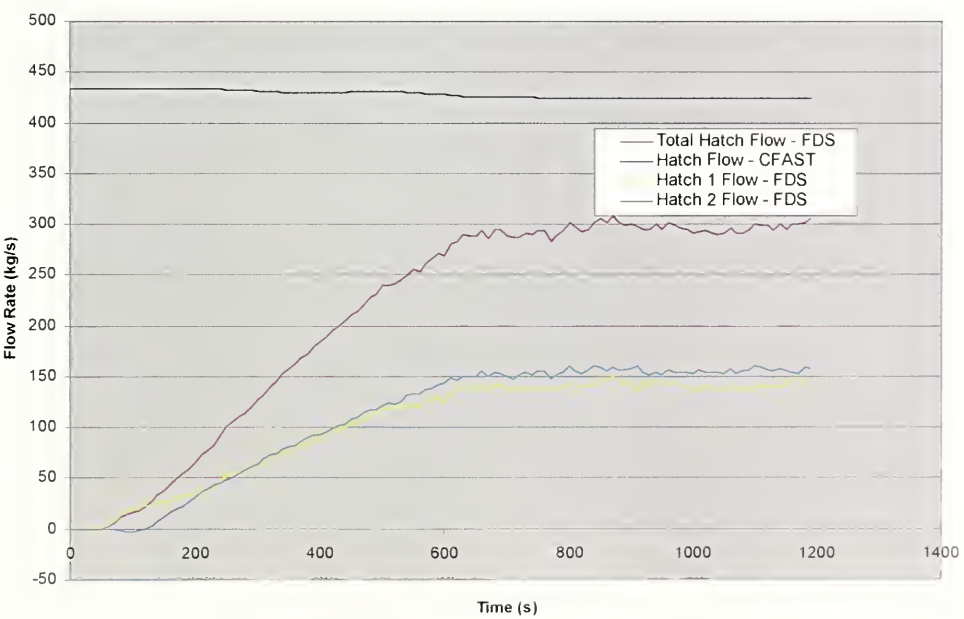

Figure 45 Hatch Flows - Case 2

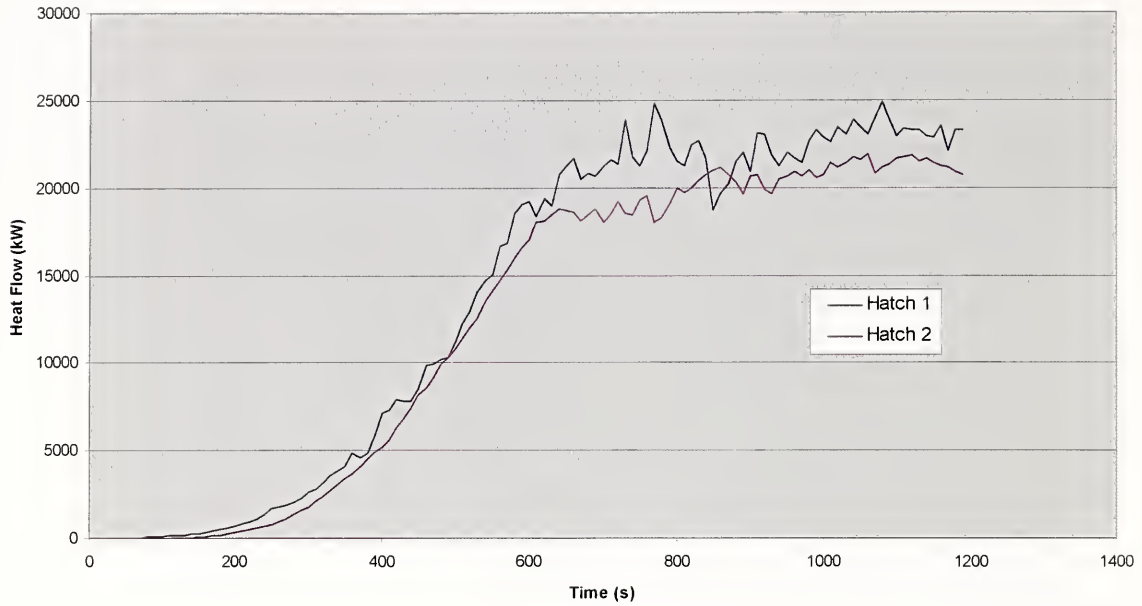

Figure 46 Hatch Heat Flows - Case 2

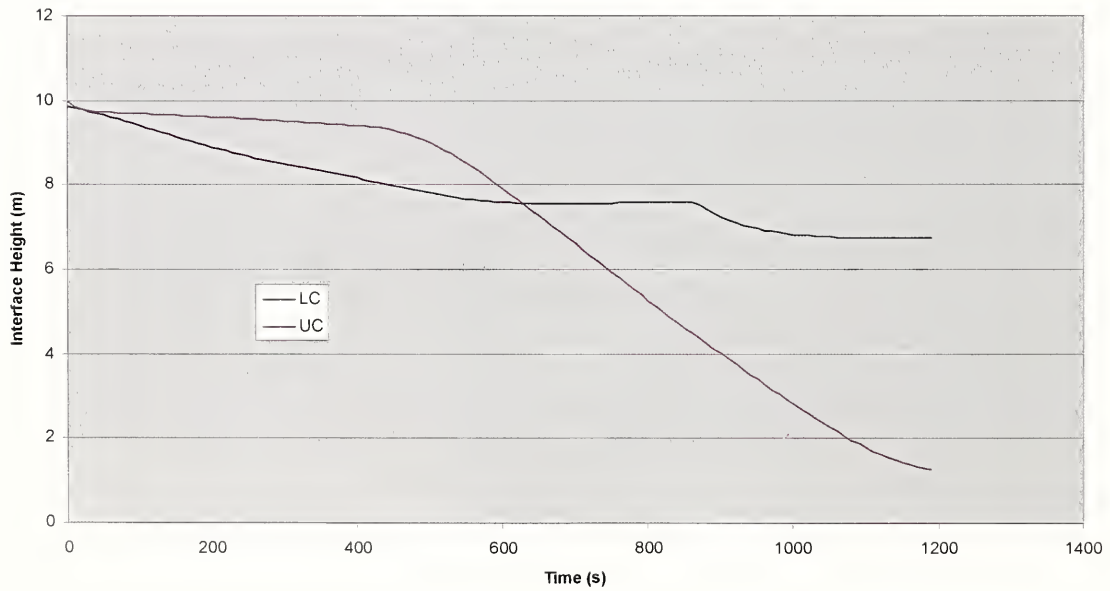

Figure 47 HGL Development (CFAST) - Case 3

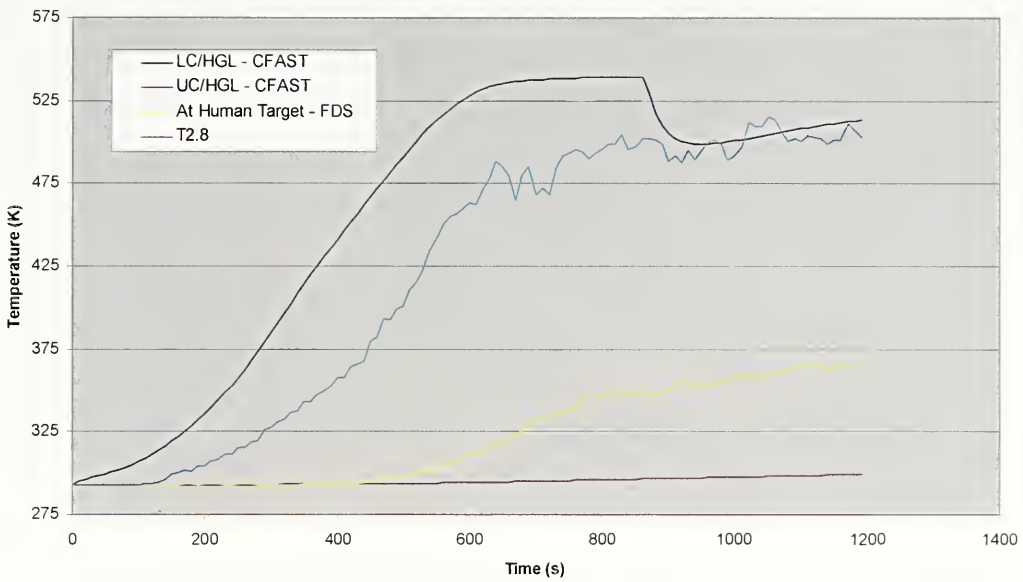

Figure 48 Gas Temperatures - Case 3

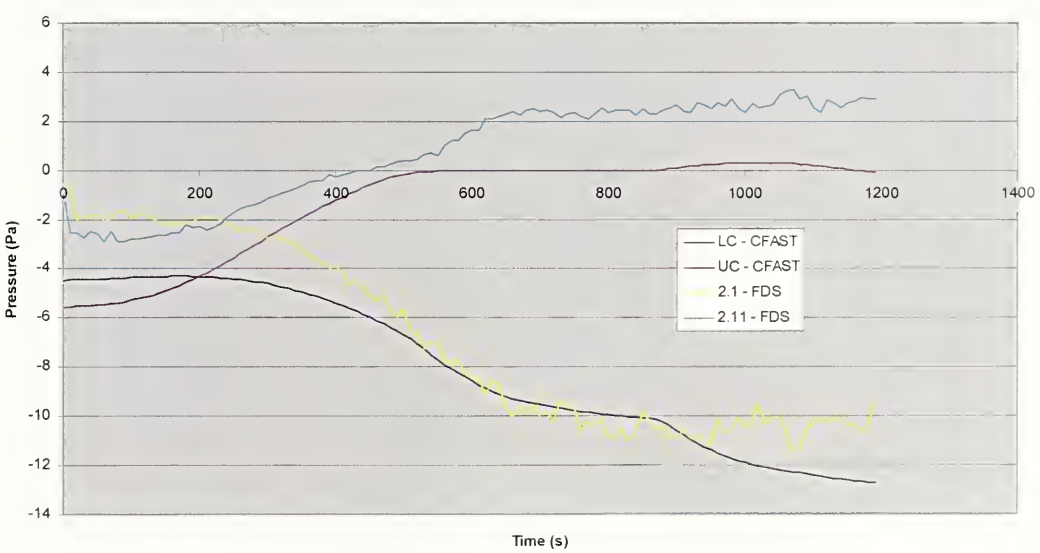

Figure 49 Pressure Development - Case 3

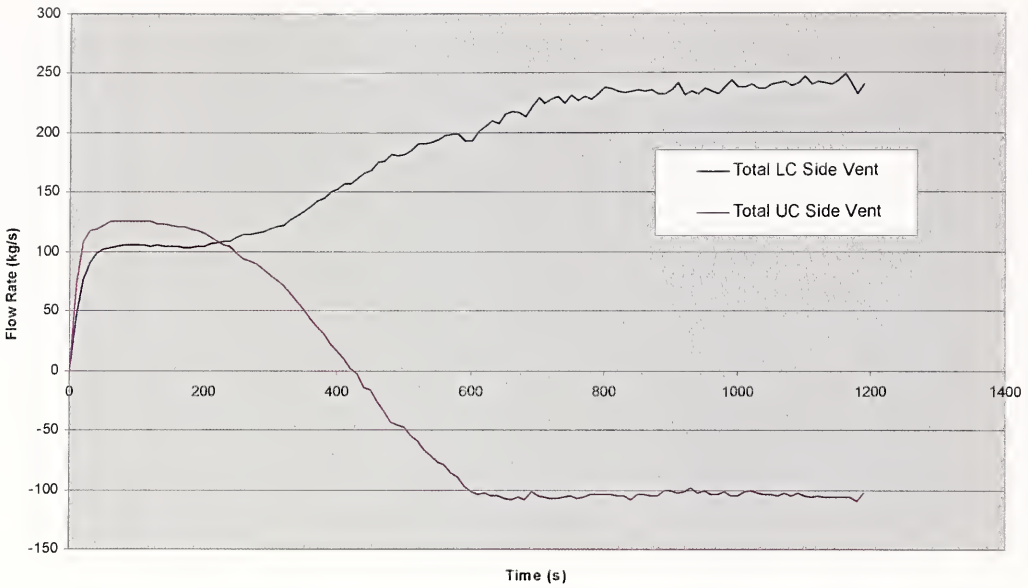

Figure 50 Vent Flows (FDS) - Case 3

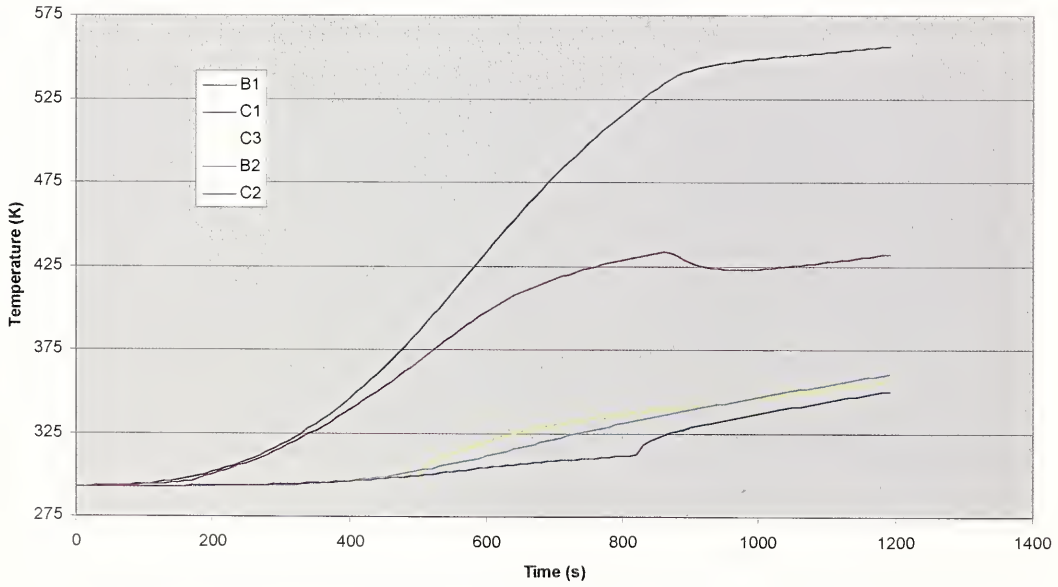

Figure 51 Target Surface Temperatures (CFAST) - Case 3

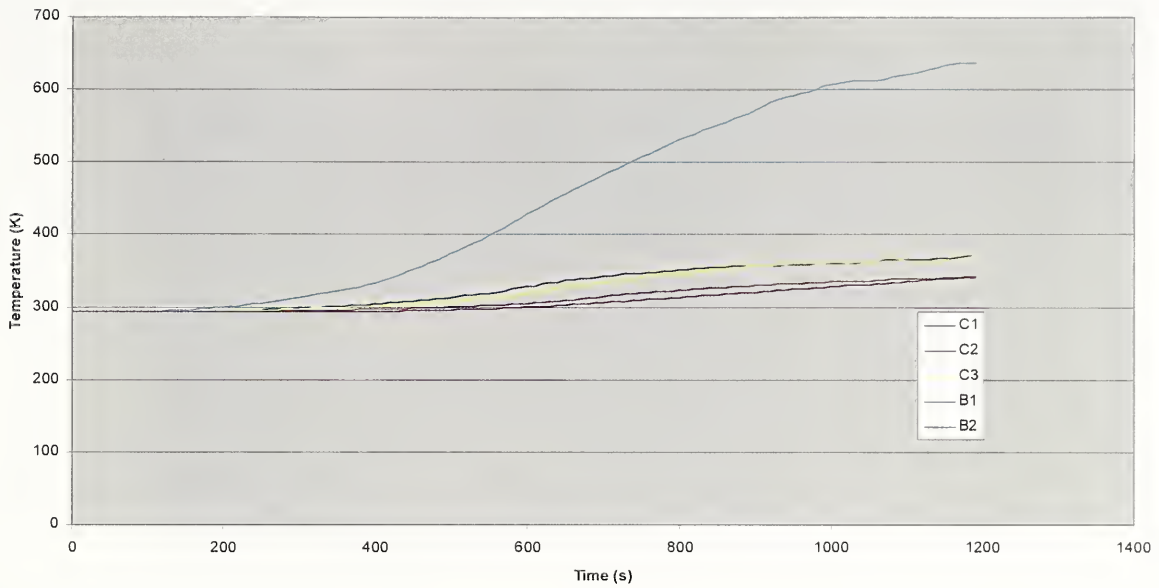

Figure 52 Target Surface Temperatures (FDS) - Case 3

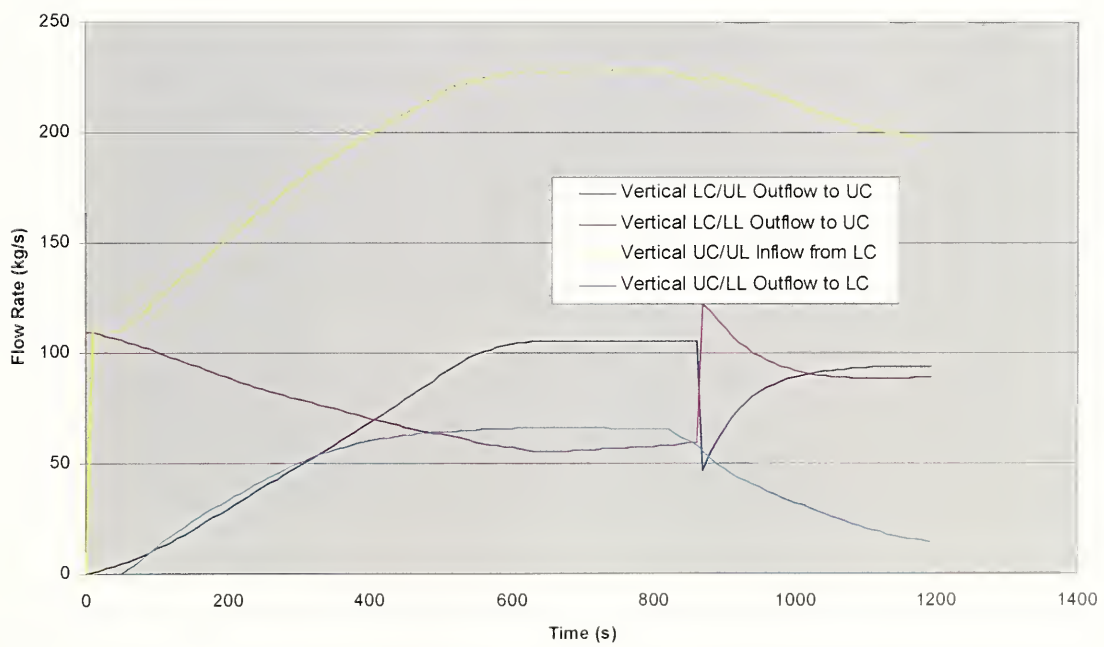

Figure 53 Hatch Flow (CFAST) - Case 3

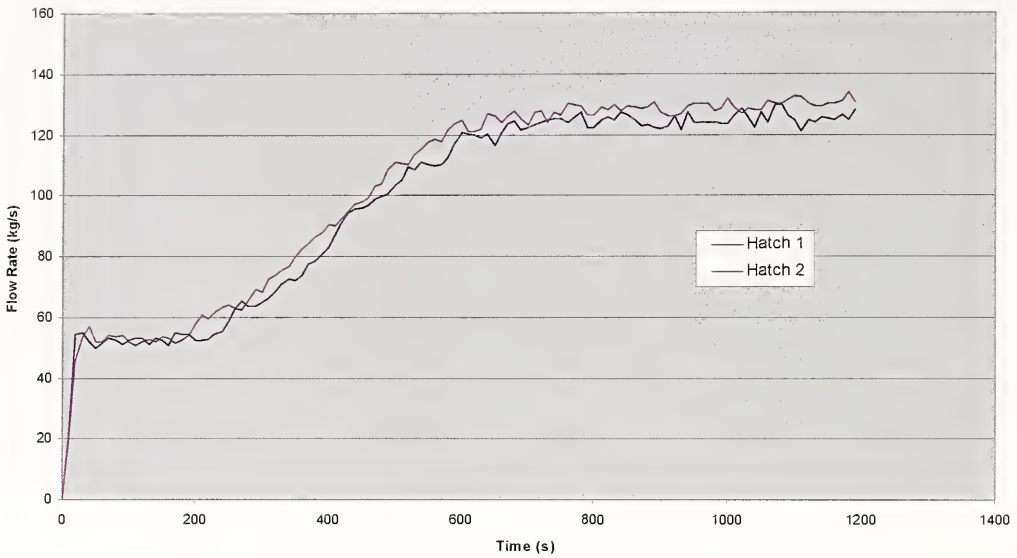

Figure 54 Hatch Mass Flows (FDS) - Case 3

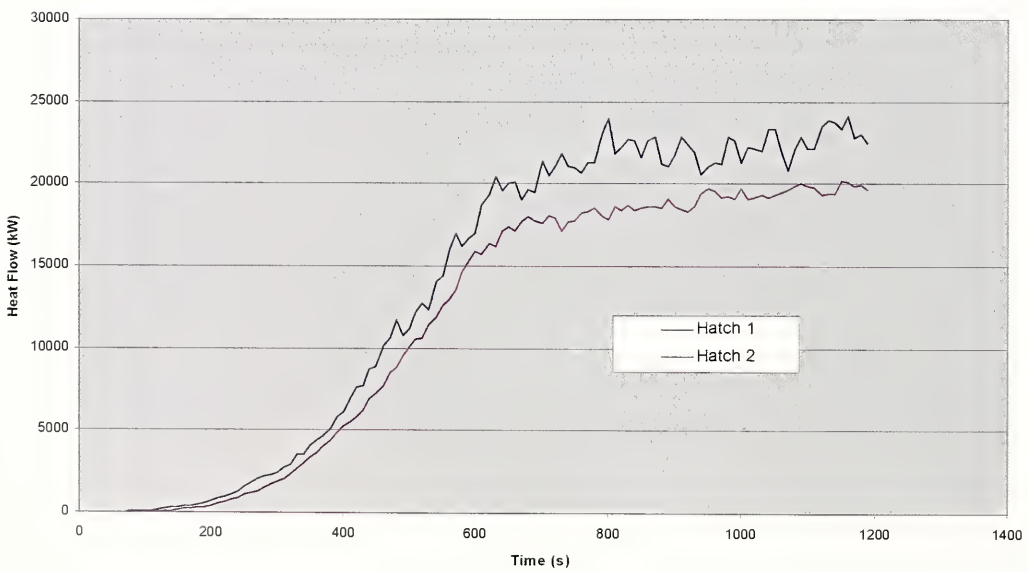

Figure 55 Hatch Heat Flows (FDS) - Case 3

5 References

Dey,M.K.,ed. "International Collaborative Project to Evaluate Fire Models for Nuclear Power Plant Applications," Summary of Planning Meeting, 24th-25th October 1999, University of Maryland, USA, NUREG/CP-0170, April 2000.

Dey, M.K., ed. "Evaluation of Fire Models for Nuclear Power Plant Applications: Cable Tray Fires - Panel Report," NUREG-1758, June 2002 and NISTIR 6872, June 2002a.

Dey, M.K., Personal communication with Jones, W.W., October 2002b.

Floyd, J.E., "Comparison of CFAST and FDS for Fire Simulation with the HDR T51 and T52 Tests," NISTIR 6866, National Institute of Standards and Technology, Gaithersburg, Maryland, March 2002.

Jones, W.W., Forney, G.P., Peacock, R.D., and Reneke, P.A., "A Technical Reference for CFAST: An Engineering Tool for Estimating Fire and Smoke Transport," NIST TN 1431, National Institute of Standards and Technology, Gaithersburg, Maryland, January 2000.

McGrattan, K.B., Baum, H.R., Rehm, R.G., Hamins, A., Forney, G.P., Floyd, J.E. & Hostikka, S. "Fire Dynamics Simulator (Version 2) - Technical Reference Guide," NISTIR 6783, National Institute of Standards and Technology, Gaithersburg, Maryland, November 2001.

McGrattan, K.B., Baum, H.R., Rehm, R.G., Hamins, A., Forney, G.P., Floyd, J.E., Hostikka, S., & Prasad, K. "Fire Dynamics Simulator (Version 3) - Technical Reference Guide," NISTIR 6783, 2002 Ed., National Institute of Standards and Technology, Gaithersburg, Maryland, November 2002.

Miles, S, "International Collaborative Project to Evaluate Fire Models for Nuclear Power Plant Applications, Specification for Benchmark Exercise # 2: Fires in a Large Hall," June 2002, Document Library <http://techconf.llnl.gov/cgi-fire/downloader/fire_models_5/006-0134.pdf>.

Mulholland, G.W., *The SFPE Handbook of Fire Protection Engineering*, Second Edition, "Smoke Production and Properties," **2**-217, Society of Fire Protection Engineering, Bethesda, Maryland, 1995.

Rockett, J.A., Keski-Rahkonen, O., & Heikkila, L, "HDR Reactor Containment Fire Modeling with BRI2, VTT Publications, 113, VTT Technical Research Center of Finland, Espoo, 1992.

Seader, J.D., & Einhorn, I.N., 16th Symp. (Int) on Combustion, Pittsburgh (1976).